



# CHORUS

This is the accepted manuscript made available via CHORUS. The article has been published as:

## Enabling adiabatic passages between disjoint regions in parameter space through topological transitions

Tiago Souza, Michael Tomka, Michael Kolodrubetz, Steven Rosenberg, and Anatoli Polkovnikov

Phys. Rev. B **94**, 094106 — Published 9 September 2016

DOI: [10.1103/PhysRevB.94.094106](https://doi.org/10.1103/PhysRevB.94.094106)

# Enabling Adiabatic Passages between Disjoint Regions in Parameter Space through Topological Transitions

Tiago Souza,<sup>1,\*</sup> Michael Tomka,<sup>1</sup> Michael Kolodrubetz,<sup>1,2,3</sup> Steven Rosenberg,<sup>4</sup> and Anatoli Polkovnikov<sup>1</sup>

<sup>1</sup>*Department of Physics, Boston University, 590 Commonwealth Ave., Boston, MA 02215, USA*

<sup>2</sup>*Department of Physics, University of California, Berkeley, CA 94720, USA*

<sup>3</sup>*Materials Sciences Division, Lawrence Berkeley National Laboratory, Berkeley, CA 94720, USA*

<sup>4</sup>*Department of Mathematics and Statistics, Boston University,*

*111 Cummington Mall, Boston, MA 02215, USA*

We explore topological transitions in parameter space in order to enable adiabatic passages between regions adiabatically disconnected within a given parameter manifold. To this end, we study the Hamiltonian of two coupled qubits interacting with external magnetic fields, and make use of the analogy between the Berry curvature and magnetic fields in parameter space, with spectrum degeneracies associated to magnetic charges. Symmetry-breaking terms induce sharp topological transitions on these charge distributions, and we show how one can exploit this effect to bypass crossing degeneracies. We also investigate the curl of the Berry curvature, an interesting but as of yet not fully explored object, which together with its divergence uniquely defines this field. Finally, we suggest a simple method for measuring the Berry curvature, thereby showing how one can experimentally verify our results.

## I. INTRODUCTION

Geometric ideas always played an important role in the understanding and unification of physical phenomena, the most prominent example demonstrating this synergy being general relativity. More recently, the discovery of topological insulators<sup>1-4</sup> brought a huge interest in the subject of topology to the field of condensed matter physics. The manifestation of geometry in quantum systems evolving adiabatically was first described by M. V. Berry<sup>5</sup> in 1984. In this seminal paper, he showed the existence of a phase with the remarkable geometric property of depending only on the path taken in parameter space and not on the rate of evolution. This geometric phase is nowadays known as the Berry phase.

We consider the case where the Hamiltonian of a system  $H(\vec{\lambda})$  depends on three real-valued parameters  $\vec{\lambda} = (\lambda^1, \lambda^2, \lambda^3)^T \in \mathbb{R}^3$ , thereby describing a three-dimensional parameter space. Focusing on the ground-state manifold, the Berry phase  $\gamma$  acquired by  $|\Psi_0(\vec{\lambda})\rangle$  after the parameters evolve adiabatically along a closed path  $C$  reads

$$\gamma(C) = \oint_C \vec{A} \cdot d\vec{\lambda} = \iint_S \vec{F} \cdot d\vec{S}, \quad (1)$$

where  $\vec{A} = i\langle\Psi_0|\vec{\nabla}|\Psi_0\rangle$  is the Berry connection. The last equality defines the Berry curvature  $\vec{F} = \vec{\nabla} \times \vec{A}$ , where the surface  $S$  is bounded by the path  $C$ . The Berry connection behaves like a  $U(1)$  gauge potential and therefore cannot directly be observed, whereas the Berry curvature is a local and gauge-invariant object manifesting the geometric properties of its associated eigenstate.

An analogy with electromagnetism (E&M), also presented by M. V. Berry<sup>5</sup>, shows that the Berry connection plays the role of a magnetic vector potential and yields through its curl the Berry curvature, which can be interpreted as an effective magnetic field. For each degeneracy

in the spectrum, one can choose a closed Gaussian surface  $\Sigma_i$  that encloses it in parameter space. The flux of the Berry curvature through  $\Sigma_i$  defines a topological quantized invariant

$$\text{ch}_1 = \frac{1}{2\pi} \iint_{\Sigma_i} \vec{F} \cdot d\vec{\Sigma}_i, \quad (2)$$

known as the first Chern number. By noting that  $\vec{\nabla} \cdot \vec{F} = \vec{\nabla} \cdot (\vec{\nabla} \times \vec{A})$ , one can see that the Berry curvature has zero divergence except at singularities. These singularities correspond to the degeneracies in the spectrum of the Hamiltonian, which play the role of effective magnetic charges in parameter space. The first Chern number quantization simply reflects the quantization of these magnetic charges. Various systems illustrating this analogy have been studied, each exhibiting different monopole charge configurations in parameter space<sup>6-13</sup>.

In this paper, we study a system of two coupled qubits which exhibits sharp topological transitions from continuous closed surfaces carrying a magnetic charge density to discrete magnetic charges in parameter space. We then show how introducing symmetry-breaking terms to the Hamiltonian, one can bypass these closed degeneracy surfaces and open adiabatic passages between topologically disjoint regions. This illustrates how one can make adiabatic transitions between different topological magnetic charge configurations. Such method allows access to the entire parameter space, and might facilitate the engineering of entangled states for quantum computation and quantum information<sup>14</sup>.

In addition, we address the issue of the previously presented analogy with E&M not being complete, since in general the Berry curvature generated by more than one degeneracy is not the same as the superposition of the effective magnetic fields of individual Berry monopoles situated at the degeneracies. The superposition principle is then not necessarily obeyed. We also present scenarios where degeneracies show a vanishing Chern number,

which is equivalent to a zero effective magnetic charge. In such cases, the curl of the Berry curvature is shown to be non-vanishing, and thus serves as a probe to identify such points experimentally. Finally, new sources akin to electric currents appear alongside the well-known magnetic charges in the curl of  $\vec{F}$ .

The paper is organized as follows. In Section II we introduce the interacting system investigated, and analyze two different scenarios in Sections III and IV, where the degeneracies of the system create disjoint regions not adiabatically connected in the parameter space. Then, in Section V, we outline how one can gain access to those forbidden regions by adiabatically breaking and reintroducing symmetries in the Hamiltonian, with topological arguments ensuring that such procedure is robust. We further discuss the symmetry-broken cases in Sections VI and VII. Finally, we present analytical and numerical analysis of a behavior repeatedly observed for all the studied cases on the curl of the Berry curvature in Section VIII, and present our conclusions in Section VIII. More detailed analytical calculations can be found in the Appendix Sections.

## II. TWO QUBIT SYSTEM

We consider a system of two interacting qubits (represented here by quantum spins  $-1/2$ ), coupled to tunable external magnetic fields. This choice was inspired by a recent experiment which measured the Berry curvature<sup>15</sup>. The Hamiltonian of the system is given by

$$H = \vec{B} \cdot (\gamma_1 \vec{\sigma}_1 + \gamma_2 \vec{\sigma}_2) + \frac{g}{2} (\sigma_1^x \sigma_2^x + \sigma_1^y \sigma_2^y) + g_z \sigma_1^z \sigma_2^z + B_0 \sigma_1^z, \quad (3)$$

where  $\vec{\sigma}_i \equiv (\sigma_i^x, \sigma_i^y, \sigma_i^z)^T$  are Pauli matrices for the  $i$ -th spin,  $\vec{B}$  is the external magnetic field acting simultaneously on both spins, anisotropically (isotropically) if  $\gamma_1 \neq \gamma_2$  ( $\gamma_1 = \gamma_2$ ),  $g$  describes the  $xy$  coupling,  $B_0$  is an offset magnetic field applied only to the first spin, breaking the exchange symmetry if non-zero, and  $g_z$  indicates the interaction in the  $z$  direction, which can turn the system into the  $SU(2)$  Heisenberg Hamiltonian for the choice of constants  $g_z = 1$ ,  $g = 2$ ,  $\gamma_1 = \gamma_2 = 1$  and  $B_0 = 0$ .

In the present analysis, we will fix  $\gamma_1$ ,  $\gamma_2$ ,  $g$ ,  $B_0$  and  $g_z$  and restrict ourselves to consider the Berry curvature with respect to the external applied magnetic field  $\vec{B} \in \mathbb{R}^3$ , defining our parameter space. The vector  $\vec{B}$  will interchangeably be written in spherical  $(B, \theta, \phi)$  or Cartesian  $(B_x, B_y, B_z) \equiv (x, y, z)$  coordinates, whichever is more convenient. The term  $g$  merely sets the energy scale, and so we will consider units in which  $g = 2$  from here onward.

The eigenenergies of (3) possess azimuthal symmetry, since the Hamiltonian and ground-state at arbitrary  $\phi$  are trivially connected to their expressions at  $\phi = 0$ . In other words,  $H(B, \theta, \phi) = R^\dagger(\phi) H(B, \theta, 0) R(\phi)$ , where

$R(\phi) = \exp(i\phi \sigma_{\text{tot}}^z/2)$ , and similarly for the ground-state,  $|\Psi_0(B, \theta, \phi)\rangle = R^\dagger(\phi) |\Psi_0(B, \theta, 0)\rangle$ . The Hamiltonian is real at  $\phi = 0$ , and therefore a gauge choice is made requiring the eigenfunctions to be real-valued. As a consequence of this gauge, the components  $A_B$  and  $A_\theta$  of the Berry connection vanish, and the only non-zero component  $A_\phi$  can be calculated explicitly (see Appendix A)

$$\vec{A} = \frac{1}{B \sin \theta} \frac{\langle \sigma_{\text{tot}}^z \rangle}{2} \hat{\phi}. \quad (4)$$

One can thus use this result to experimentally measure the Berry connection by measuring the ground-state expectation value of the total magnetization, with the Berry curvature obtained by taking the curl of Eq. (4).

In analogy with E&M, one of Maxwell's equations in  $\mathbb{R}^3$  for the vector field  $\vec{F}$  is

$$\vec{\nabla} \cdot \vec{F} = 2\pi\rho_m, \quad (5)$$

with  $\rho_m$  denoting the effective magnetic charge density. The expression above is nothing but the differential form of Eq. (2), showing that the divergence of  $\vec{F}$  is equal to the effective magnetic charge (first Chern number). The role of Chern numbers as topological quantifiers in quantum systems has been widely investigated, and it is still a very active field<sup>16,17</sup>. A direct measurement of the Berry curvature was proposed in<sup>18,19</sup>, where it was shown to be given by the non-adiabatic response of certain physical observables. This was experimentally confirmed with systems of superconducting qubits<sup>15,20</sup>, where the first Chern number quantization was readily confirmed.

However, the role of  $\vec{\nabla} \times \vec{F}$  has not been explored so far. In three-dimensional space, any vector field is uniquely represented by its divergence and curl. The divergence of  $\vec{F}$ , as seen from Eq. (5), is given by effective magnetic charges, while the curl is analogous to "electric" currents. In what follows, we then study in detail the divergence and curl of  $\vec{F}$  for different fixed set of values of the parameters  $\gamma_1, \gamma_2, g_z$  and  $B_0$ . We start with the choice that makes the Hamiltonian (3)  $SU(2)$  symmetric, and break symmetries in each subsequent case.

## III. HEISENBERG INTERACTION

The simplest system extending the aforementioned E&M analogy to continuous magnetic charge densities has the Hamiltonian  $H = \vec{B} \cdot (\vec{\sigma}_1 + \vec{\sigma}_2) + \vec{\sigma}_1 \cdot \vec{\sigma}_2$ . A similar system and its charge configuration was studied in<sup>6</sup>. Ours corresponds to the two-spin Heisenberg model in an external  $\vec{B}$  field, possessing  $SU(2)$  symmetry. It is obtained from the Hamiltonian (3) by setting the parameters to  $\gamma_1 = \gamma_2 = g_z = 1$ ,  $B_0 = 0$ .

The ground-state degenerates on the sphere of radius  $B = 2$ , dividing the parameter space into two disjoint regions. The Berry curvature in this case is

$$\vec{F} = \begin{cases} 0, & B < 2, \\ \frac{1}{2} q_m \frac{\hat{B}}{B^2}, & B > 2, \end{cases} \quad (6)$$

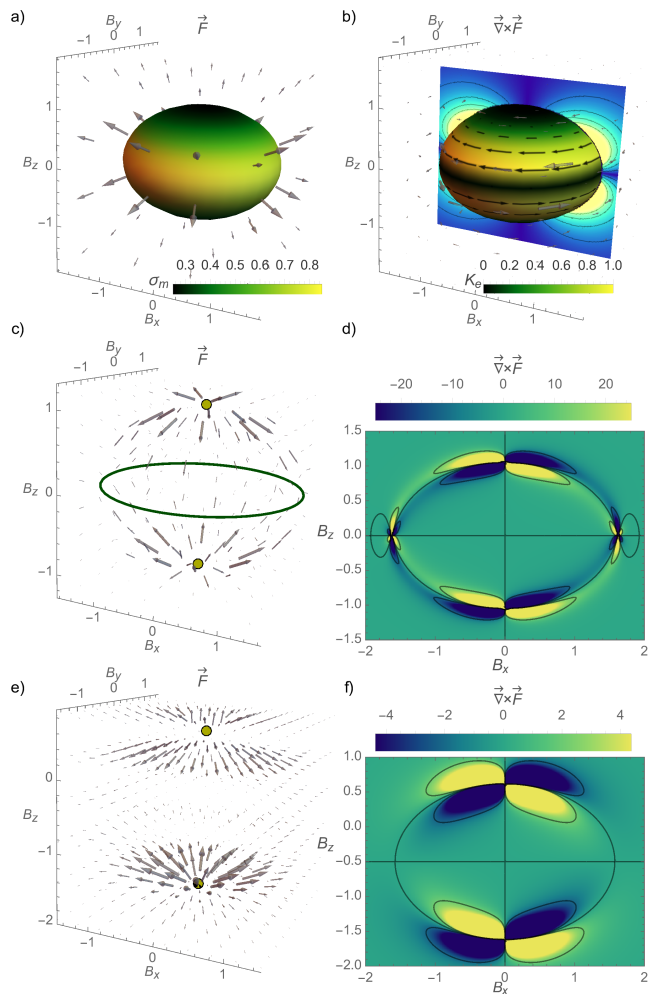


FIG. 1. *XXZ-interaction* ( $g_z = 0$ ): a) Berry curvature  $\vec{F}$  (light arrows) and magnetic surface charge density  $\sigma_m$  (color bar). b)  $\vec{\nabla} \times \vec{F}$ , with magnitude shown in the  $xz$ -plane. The curl has only a  $\phi$  component, and the colors on the ellipsoid illustrate the magnitude of the electric surface current density  $\vec{K}_e = K_e \hat{\phi}$ , with direction indicated by the darker arrows. *Anisotropic fields* ( $g_z = 0$ ,  $\alpha = 0.3$ ): c) Berry curvature  $\vec{F}$  (light arrows), showing two charges (yellow dots) on the  $z$ -axis, plus an uncharged ring (green) in the  $xy$ -plane. d) The curl of the Berry curvature, shown only in the  $xz$ -plane since it has azimuthal symmetry. *Broken exchange symmetry* ( $g_z = 0$ ,  $\alpha = 0$ ,  $B_0 = 1$ ): e) Berry curvature  $\vec{F}$  (light arrows) showing now the only two magnetic charges on the  $z$ -axis. f)  $\vec{\nabla} \times \vec{F}$  shown in the  $xz$ -plane.

where  $q_m = 2$  gives the effective magnetic charge (see Appendix B). The effective magnetic field defined by the Berry curvature above is akin to the electric field of a hollow conducting sphere of radius two. The total magnetic charge is equal to the Chern number,  $\text{ch}_1 = 2$ , and can be obtained from Eq. (2). The magnetic charge density distribution  $\rho_m$  is uniform since the sphere is a surface of constant curvature. The curl of  $\vec{F}$  is equal to zero since the field falls off radially as  $1/B^2$ . This will not be the case in the following examples.

#### IV. XXZ INTERACTION

Let us now consider the case where  $g_z \neq 1$ , and as before,  $\gamma_1 = \gamma_2 = 1$ ,  $B_0 = 0$ . Unlike the Heisenberg case, if  $|g_z| < 1$  ( $|g_z| > 1$ ) we find that the  $SU(2)$  symmetry is broken, and the charged sphere of the prior case gets continuously squeezed (stretched) along the  $z$ -axis, becoming an oblate (prolate) ellipsoid of revolution. In analogy to the charge distribution on conductors in electrostatics, the magnetic charge density is no longer uniformly distributed, but accumulates in regions of higher curvature (see Fig. 1a). In spite of the non-uniform surface charge density, the total charge on the entire surface remains the same as for the previous case ( $\text{ch}_1 = 2$ ). This can be concluded from the fact that the ground-state remains fully polarized at large  $B$ , yielding the total effective charge enclosed as a topologically protected integer equal to  $\text{ch}_1 = 2$ .

Figure 1b shows the existence of a surface current  $\vec{K}_e \neq 0$  defined by the discontinuity of the parallel component of  $\vec{F}$  across the surface, which implies that  $\vec{\nabla} \times \vec{F} \neq 0$  (see Appendix C). The Berry curvature has only  $\hat{B}$  and  $\hat{\theta}$  components, and therefore its curl is parallel to  $\hat{\phi}$ . The non-uniform magnetic charge distribution produces a quadrupole in the curl of  $\vec{F}$ .

In the previous two cases we have explored situations of high symmetry, where the magnetic charges occur as surface densities spread on closed degeneracy surfaces, instead of the more commonly studied discrete monopole charges<sup>5</sup>. Similar cases of continuous surfaces with magnetic charge densities have been explored elsewhere<sup>6</sup>. The newest aspect of the aforementioned results is shown by the curl of the Berry curvature, which displays a characteristic quadrupole pattern.

#### V. BYPASSING DEGENERACY CROSSINGS

The points belonging to the closed surfaces in the two previous cases indicate the locus in parameter space where there are degeneracies in the ground-state. Interestingly, inside all the previous surfaces, the ground-state is a singlet  $|\Psi_0\rangle \equiv \frac{1}{\sqrt{2}}(|\uparrow\downarrow\rangle - |\downarrow\uparrow\rangle)$ , i.e., a Bell entangled state of the two qubits (see Appendixes B & C). Equation (4) then implies a vanishing Berry connection and curvature; in the region outside the closed surfaces,  $|\Psi_0\rangle$  has contributions of the other vectors in the spin-product basis. At first sight, it might seem impossible to experimentally start with a high polarizing field  $B_z \gg B_x \approx 0$  where  $|\Psi_0\rangle \approx |\uparrow\uparrow\rangle$  to subsequently prepare adiabatically a pure singlet-state without crossing the continuous degeneracy surface, which would introduce excitations and break the adiabaticity.

In order to bypass this topological constraint, we now consider situations with significantly reduced symmetry, and we observe a sharp collapse of the surface charge density to the more familiar case of magnetic monopoles.

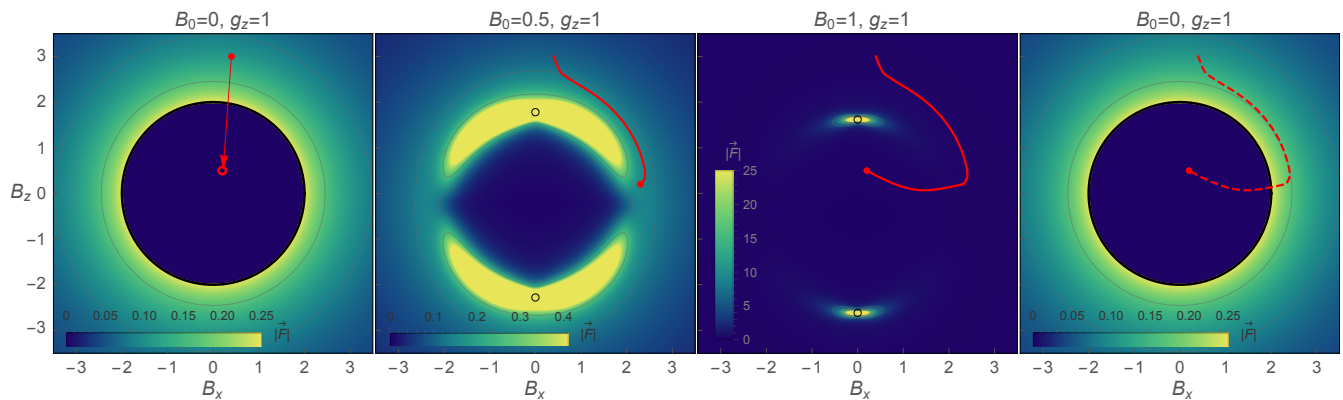


FIG. 2. *Opening an adiabatic passage between topologically disjoint regions in parameter space.* First panel: starting with a point in parameter space corresponding to a state outside the sphere defined by the Heisenberg Hamiltonian. Second and third panel: Breaking symmetry by adiabatically introducing a pinning field in one of the spins creates a different topological magnetic charge distribution (with the total magnetic charge conserved). One can now evolve the system to a previously adiabatically inaccessible region. Fourth panel: Reintroducing the symmetry by removing the symmetry-breaking term allows one to bypass the continuous crossing surface and enter a previously adiabatically disconnected region in parameter space.

This singular change in the topology of the monopole charge density is unlike anything in classical E&M, and we explore this phase transition to open a passage and access the interior regions of the previous cases by adiabatically breaking and reestablishing symmetries (see Fig. 2). We also show how the effective electromagnetic fields respond to this transition.

## VI. ANISOTROPIC FIELDS

Anisotropy is introduced by setting  $\gamma_1 = 1 + \alpha$ ,  $\gamma_2 = 1 - \alpha$  with  $\alpha \neq 0$  and  $g_z = B_0 = 0$ . The introduction of  $\alpha$  breaks the symmetry that allows the existence of a two-dimensional manifold where the ground-state degeneracies occurs. The previous surfaces now collapse to two points, located on the  $z$ -axis at  $\pm g/(2\sqrt{1-\alpha^2})$  due to azimuthal symmetry of the eigenenergies. These two points correspond to energy level crossings in the ground-state manifold and act like sources of  $\vec{F}$ . The total Chern number in the entire parameter space is topologically protected and equal to  $+2$ , therefore each source carries an effective magnetic charge equal to  $+1$ .

These magnetic monopoles are visible as singularities in the divergence of the Berry curvature, which is unsurprisingly zero away from these two singularities. For the curl of the Berry curvature, we find a quadrupolar field pattern very similar to what we saw in the previous section for the charged surface. However, surprisingly we also find the appearance of two other points on the  $x$ -axis. Respecting the model's symmetry by revolving the plotted planes around the  $z$ -axis, one can see that these points in fact correspond to a ring of degeneracies, centered at the origin in the  $xy$ -plane, with radius  $\rho = \sqrt{2(1+\alpha^2)}/(1-\alpha^2)$  (see Fig. 1c). Most interestingly, this ring is uncharged as can be inferred from a topological argument: the total Chern number

for the entire parameter manifold must remain equal to  $+2$ , and the monopoles on the  $z$ -axis each carries a unit charge, as can be verified using Gauss law. The Berry curvature in its vicinity exhibits a saddle-point behavior, rather than acting like a sink or source for the  $\vec{F}$  vector field. The analogous configuration in E&M are two electric charges with a conducting ring placed halfway in between, which introduces boundary conditions for the fields. As can be seen in Fig. 1c, the curl of Berry curvature shows a hexapole pattern for the intersections on the  $xy$ -plane. Thus, the presence of the uncharged ring, although not obvious from the Berry curvature field, can clearly be observed in the  $\vec{\nabla} \times \vec{F}$  graph, as they exhibit a distinct pattern compared to degeneracies having an effective charge. The curl then apparently contains additional geometric information about the ground-state manifold of the system, which has not been explored so far.

It is readily confirmed that the gap vanishes at this ring of singularities despite the absence of effective magnetic charge. Interestingly, crossing this degeneracy by fixing  $B_x = \rho$  and varying  $B_z$ , we find that the energies exhibit a quadratic touching, which in the chemistry literature is known as Renner-Teller intersection points<sup>6,21-23</sup>, fundamentally different from conical intersections since they do not give rise to a geometric phase, and consequently have a Chern number equal to 0. This quadratic touching comes from a symmetry of the Hamiltonian, namely  $B_z \rightarrow -B_z$ , and therefore is not present for curves that do not cross the degeneracy vertically, e.g., the energy levels for fixed  $B_z = 0$  when varying  $B_x$ .

## VII. BROKEN EXCHANGE SYMMETRY

For the final case, consider  $\gamma_1 = \gamma_2 = 1$ ,  $g_z = 0$  and  $B_0 = 1$ . Due to the pinning field  $B_0$  on the first spin

the exchange symmetry between the two spins is broken, and only the azimuthal symmetry in the eigenenergies is left. The crossing points now lie solely on the  $z$ -axis, with the two monopoles located at  $B_z^{(\pm)} \equiv (-B_0 \pm \delta)/2$ , where  $\delta \equiv \sqrt{B_0^2 + g^2}$  is the degenerate ground-state energy for the case in consideration. The curl of  $\vec{F}$  for this case shows a persistent quadrupole pattern around the crossing points in the  $z$ -axis, although one observes a bending of the lobes toward each other, which increases with  $B_0$  (see Fig. 1e). The point charges along the  $z$ -axis are no longer symmetric with respect to the  $xy$ -plane, and their location varies as a function of  $B_0$ , given by  $B_z^{(\pm)}$ .

### VIII. CURL ANALYSIS

To understand the curl behavior of  $\vec{F}$  analytically, we calculate the Berry connection for the broken exchange symmetry case at the degeneracy points  $B_z^{(\pm)}$  using perturbation theory and obtain  $\vec{\nabla} \times \vec{F}$  around  $B_z^{(\pm)}$  (see Appendix E). The leading order expression for the curl is given by

$$\vec{\nabla} \times \vec{F}_{(\pm)} = -\frac{3}{4} \frac{\beta^2 \sin 2\vartheta}{\gamma^2 (1 - \beta^2 \sin^2 \vartheta)^{5/2}} \frac{1}{dB^3} \hat{\phi} + \dots, \quad (7)$$

where  $\beta^2 \equiv g/\delta$ ,  $\gamma \equiv 1/\sqrt{(1 - \beta^2)}$ , and with respect to the coordinate system centered at the monopole  $B_z^{(\pm)}$  respectively, given in spherical coordinates  $(dB, \vartheta, \phi)$ . This expression reproduces qualitatively the quadrupole seen numerically (see Fig. 1d and Appendix F) and suggests the possibility that this pattern may be robust in the vicinity of Berry curvature sources.

### IX. CONCLUSION

The analogy between E&M and degeneracies in quantum systems has been outlined many years ago, and it is still a field of active research, mainly due to its applications to adiabatic quantum computing and the recent burst of interest in topological transitions. For highly symmetric systems, we have shown how symmetry-breaking perturbations allows one to open adiabatic passages in previously topologically disjoint regions, thereby allowing the full parameter space to be explored. The procedure outlined in this paper is general and robust, and not necessarily restricted to qubits. We note that by identifying angles of the magnetic field with quasi-momenta, the two-spin system here analyzed can be mapped to a four-band model of a topological insulator with a rich phase diagram, similar to the construction in<sup>15</sup>. Therefore results presented in this paper can find direct analogues in other systems. The system in analysis was chosen as a good illustrative example due to experimental feasibility of measuring the Berry connection

$\vec{A}$  by relating it to the ground-state expectation value of the total magnetization. The Berry curvature and its curl can then be experimentally obtained, and the results here presented can be verified.

We also highlighted the existence of degeneracy points with vanishing Chern number, and exemplified how they fit within the E&M analogy as boundary conditions for the  $\vec{F}$  field. Finally, the curl of the Berry curvature was explored, with different behavior near charged and uncharged points, indicating the possibility that this quantity might carry geometrical information about the ground-state manifold previously unexplored.

### ACKNOWLEDGMENTS

The authors thank P. Roushan, A. Dunsworth and T. Pudlik for enlightening discussions. T. S. and A. P were supported by AFOSR FA9550-13-1-0039, NSF DMR-1506340, ARO W911NF1410540. M. T. was funded by the Swiss National Science Foundation (SNSF), M. K. was supported by Laboratory Directed Research and Development (LDRD) funding from Berkeley Lab, provided by the Director, Office of Science, of the U.S. Department of Energy under Contract No. DE-AC02-05CH11231.

#### Appendix A: Locations of the effective magnetic charges for an interacting two qubit system

In the main text, we plot the Berry curvature and its curl for the ground-state  $|\Psi_0\rangle$  to illustrate the locations of the ground-state degeneracies in parameter space. We use the analogy with electromagnetism, pointed out by M. V. Berry<sup>5</sup>, that identifies the Berry curvature  $\vec{F}$  with an effective magnetic field in parameter space whose vector potential is the Berry connection  $\vec{A} = i\langle\Psi_0|\vec{\nabla}|\Psi_0\rangle$ . The locations of the associated magnetic charges are given by the ground-state degeneracies, and their charge is determined by the first Chern number. The fact that degeneracies of the ground-state act as magnetic charges can be seen by the following reasoning: the vector identity  $\vec{\nabla} \cdot (\vec{\nabla} \times \vec{A}) = 0$  holds only if  $\vec{A}$  has continuous derivatives. This is no longer the case when the ground-state becomes degenerate, since at these points  $|\Psi_0\rangle$  undergoes a discontinuous change and so the derivatives of  $\vec{A}$  become discontinuous. As a result, at the degeneracies we have  $\vec{\nabla} \cdot (\vec{\nabla} \times \vec{A}) \neq 0$ , and in analogy with Maxwell's equations we can write an equivalent Gauss's law for the Berry curvature

$$\vec{\nabla} \cdot \vec{F} = 2\pi\rho_m, \quad (A1)$$

where  $\rho_m$  is the effective magnetic charge density. The volume integral of (A1) yields

$$\iint_{\Sigma} \vec{F} \cdot d\vec{S} = 2\pi \iiint_V \rho_m dV, \quad (A2)$$

where the divergence theorem was applied to the left hand side of the equation. According to the Chern theorem<sup>24</sup>, the integral of the Berry curvature over a closed manifold  $\Sigma$  is quantized in units of  $2\pi$ , and this number defines the first Chern number

$$\text{ch}_1 = \frac{1}{2\pi} \iint_{\Sigma} \vec{F} \cdot d\vec{S}. \quad (\text{A3})$$

The comparison of the previous two equations implies the quantization of  $\iiint_V \rho_m dV$ , which also defines the effective charge enclosed by the manifold  $\Sigma$ .

For a single magnetic monopole charge  $q_m$ , the magnetic charge density is  $\rho_m = q_m \delta(\vec{r})$  and the associated magnetic field is then given, in view of Eq. (A2), by

$$\vec{F} = \frac{1}{2} q_m \frac{\hat{r}}{|\vec{r}|^2}, \quad (\text{A4})$$

where the prefactor of  $1/2$  sets the units such that the charge  $q_m$  is equal to the Chern number. This example is realized by a single qubit (spin-1/2) in an external magnetic field  $\vec{B}$ , where the resulting Berry curvature is given by (A4) and therefore analogous to an effective magnetic field in parameter space  $(B_x, B_y, B_z)$ , or  $\vec{r} \equiv \vec{B}$ , created by a magnetic monopole sitting at  $B = 0$  and carrying a charge  $q_m = 1$ .

Finally, we note that the Berry curvature  $\vec{F}$  associated with the ground-state can also be rewritten, using the resolution of the identity  $\sum_m |\Psi_m\rangle\langle\Psi_m| = 1$ , as a sum over all other eigenstates

$$\vec{F} = i \sum_{m \neq 0} \frac{\langle\Psi_0|\vec{\nabla}H|\Psi_m\rangle \times \langle\Psi_m|\vec{\nabla}H|\Psi_0\rangle}{(E_0 - E_m)^2}. \quad (\text{A5})$$

This equation highlights that degeneracies in the ground-state,  $E_0 = E_m$ , act as charges for  $\vec{F}$ . In particular, the expression (A5) is useful to compute the Berry curvature numerically, if the Hamiltonian is not analytically diagonalizable.

In the following, we illustrate the calculations that lead to the localization of the ground-state degeneracies in parameter space for the two-qubit systems considered in the main text. We also calculate the corresponding Berry connection, curvature and its curl. First, however, let us review some important properties of the system studied in the main text, consisting of two interacting qubits, with each qubit separately coupled to external magnetic fields. The Hamiltonian of this system is given by

$$H = \vec{B} \cdot (\gamma_1 \vec{\sigma}_1 + \gamma_2 \vec{\sigma}_2) + \frac{g}{2} (\sigma_1^x \sigma_2^x + \sigma_1^y \sigma_2^y) + g_z \sigma_1^z \sigma_2^z + B_0 \sigma_1^z, \quad (\text{A6})$$

where  $\vec{\sigma}_i \equiv (\sigma_i^x, \sigma_i^y, \sigma_i^z)^T$  are the usual Pauli matrices for the  $i$ -th spin

$$\sigma_i^x = \begin{pmatrix} 0 & 1 \\ 1 & 0 \end{pmatrix}, \quad \sigma_i^y = \begin{pmatrix} 0 & -i \\ i & 0 \end{pmatrix}, \quad \sigma_i^z = \begin{pmatrix} 1 & 0 \\ 0 & -1 \end{pmatrix}, \quad (\text{A7})$$

with  $i = 1, 2$ . The external magnetic field is  $\vec{B} = (B_x, B_y, B_z)^T \equiv (x, y, z)^T$ , which acts isotropically on both spins if  $\gamma_1 = \gamma_2$ , and anisotropically if  $\gamma_1 \neq \gamma_2$ . The field  $B_0$  is a local magnetic field applied only to the first spin in the  $z$  direction, and allows us to break the exchange symmetry between the two spins. The term  $g$  is the energy scale of the interaction between the two spins in the  $x$  and  $y$  direction, and  $g_z$  indicates the interaction in the  $z$  direction.

As mentioned in the main text, we consider the parameters  $\gamma_1, \gamma_2, g, B_0$  and  $g_z$  as fixed and restrict ourselves to the case of an adiabatically varying external magnetic field  $\vec{B}$  that spans the parameter space  $\mathcal{M} \equiv \mathbb{R}^3$ . The magnetic field  $\vec{B}$  in spherical coordinates  $(B, \theta, \phi)$  reads  $\vec{B} = B (\sin \theta \cos \phi, \sin \theta \sin \phi, \cos \theta)^T = B \hat{B}(\theta, \phi)$ , where  $\hat{B}(\theta, \phi)$  is the unit vector in the radial direction. The Hamiltonian in spherical coordinates can be rewritten as

$$H(B, \theta, \phi) = B \hat{B}(\theta, \phi) \cdot (\gamma_1 \vec{\sigma}_1 + \gamma_2 \vec{\sigma}_2) + \frac{g}{2} (\sigma_1^x \sigma_2^x + \sigma_1^y \sigma_2^y) + g_z \sigma_1^z \sigma_2^z + B_0 \sigma_1^z, \quad (\text{A8})$$

and written in this form, it is evident that the Hamiltonian at arbitrary  $\phi$  can be obtained from the one at  $\phi = 0$  by

$$H(B, \theta, \phi) = R^\dagger(\phi) H(B, \theta, 0) R(\phi), \quad (\text{A9})$$

where  $R(\phi) = \exp(i\phi \sigma_{\text{tot}}^z/2)$  and  $\sigma_{\text{tot}}^z = \sigma_1^z + \sigma_2^z$ . Equation (A9) implies that the eigenstates of  $H(B, \theta, \phi)$  are simply given by a rotation of the eigenstates of  $H(B, \theta, 0)$ ,

$$|\Psi_m(B, \theta, \phi)\rangle = R^\dagger(\phi) |\Psi_m(B, \theta, 0)\rangle, \quad (\text{A10})$$

and that the eigenenergies of  $H(B, \theta, \phi)$  and  $H(B, \theta, 0)$  are the same,  $E_m(B, \theta, \phi) = E_m(B, \theta, 0)$ . Note that Eq. (A9) does not provide any additional conservation laws but it is useful for the calculation of the Berry connection and curvature.

We emphasize that the Berry connection is a connection one-form on the parameter space  $\mathcal{M}$ , in general defined by  $A \equiv i\langle\Psi_0|d|\Psi_0\rangle$ , where  $d$  is the exterior derivative. The corresponding Berry curvature is a two-form defined by  $F = dA$ . In local coordinates  $(x^1, x^2, \dots)$  we can write

$$A = A_\mu dx^\mu, \quad A_\mu = i\langle\Psi_0|\partial_\mu|\Psi_0\rangle, \quad (\text{A11})$$

and where  $\partial_\mu = \frac{\partial}{\partial x^\mu}$ ,  $\mu = 1, 2, \dots$ . Similarly, the Berry curvature in local coordinates reads

$$F = \frac{1}{2} F_{\mu\nu} dx^\mu \wedge dx^\nu, \quad F_{\mu\nu} = \partial_\mu A_\nu - \partial_\nu A_\mu, \quad (\text{A12})$$

where  $dx^\mu \wedge dx^\nu$  is the wedge product of two one-forms. For a three dimensional parameter space  $\mathcal{M}$  as the one studied in the main text, the components of the Berry connection one-form  $A_\mu$  can be collected in a vector as  $\vec{A} = i\langle\Psi_0|\vec{\nabla}|\Psi_0\rangle$ . Similar, the Berry curvature two-form can be mapped to a vector through  $\vec{F} = \vec{\nabla} \times \vec{A}$ . This

mapping can be seen explicitly from the definition of the Berry curvature in local coordinates  $F_{\mu\nu} = \partial_\mu A_\nu - \partial_\nu A_\mu$ , which is an antisymmetric tensor. In three dimensions, it reduces to

$$(F_{\mu\nu}) = \begin{pmatrix} F_{11} & F_{12} & F_{13} \\ F_{21} & F_{22} & F_{23} \\ F_{31} & F_{32} & F_{33} \end{pmatrix} \equiv \begin{pmatrix} 0 & F_3 & -F_2 \\ -F_3 & 0 & F_1 \\ F_2 & -F_1 & 0 \end{pmatrix} \quad (\text{A13})$$

and thus we can write  $\vec{F} = (F_1, F_2, F_3)^T = (F_{23}, F_{31}, F_{12})^T$ .

In view of the discussion in the previous paragraph the Berry connection in Cartesian coordinates,  $(B_x, B_y, B_z) \equiv (x, y, z)$ , reads

$$\vec{A}^{(C)}(x, y, z) = A_x \hat{x} + A_y \hat{y} + A_z \hat{z}, \quad (\text{A14})$$

where  $A_\mu = i \langle \Psi_0 | \partial_\mu | \Psi_0 \rangle$ , with  $\mu = \{x, y, z\}$ ,  $\partial_\mu = \frac{\partial}{\partial \mu}$ , and  $\hat{x}$ ,  $\hat{y}$  and  $\hat{z}$  are the unit vectors in Cartesian coordinates. One should be wary, since there is a potential for ambiguity in this notation if a different choice of coordinate system is considered. For example, with respect to spherical coordinates  $(B, \theta, \phi)$ , the Berry connection becomes

$$\vec{A}^{(S)}(B, \theta, \phi) = A_B \hat{B} + A_\theta \hat{\theta} + A_\phi \hat{\phi}, \quad (\text{A15})$$

where now we must define

$$\begin{aligned} A_B &= i \langle \Psi_0 | \partial_B | \Psi_0 \rangle \\ A_\theta &= i \frac{1}{B} \langle \Psi_0 | \partial_\theta | \Psi_0 \rangle \\ A_\phi &= i \frac{1}{B \sin \theta} \langle \Psi_0 | \partial_\phi | \Psi_0 \rangle \end{aligned} \quad (\text{A16})$$

since in spherical coordinates the operator  $\vec{\nabla}$  is given by

$$\vec{\nabla} f = \frac{\partial f}{\partial B} \hat{B} + \frac{1}{B} \frac{\partial f}{\partial \theta} \hat{\theta} + \frac{1}{B \sin \theta} \frac{\partial f}{\partial \phi} \hat{\phi}, \quad (\text{A17})$$

where

$$\begin{aligned} \hat{B} &= \sin \theta \cos \phi \hat{x} + \sin \theta \sin \phi \hat{y} + \cos \theta \hat{z} \\ \hat{\theta} &= \cos \theta \cos \phi \hat{x} + \cos \theta \sin \phi \hat{y} - \sin \theta \hat{z} \\ \hat{\phi} &= -\sin \phi \hat{x} + \cos \phi \hat{y} \end{aligned} \quad (\text{A18})$$

are the local orthogonal unit vectors in the directions of increasing  $B$ ,  $\theta$  and  $\phi$ , respectively. Note that the Cartesian unit vectors can be expressed as

$$\begin{aligned} \hat{x} &= \sin \theta \cos \phi \hat{B} + \cos \theta \cos \phi \hat{\theta} - \sin \phi \hat{\phi} \\ \hat{y} &= \sin \theta \sin \phi \hat{B} + \cos \theta \sin \phi \hat{\theta} + \cos \phi \hat{\phi} \\ \hat{z} &= \cos \theta \hat{B} - \sin \theta \hat{\theta} \end{aligned} \quad (\text{A19})$$

or the spherical unit vectors as

$$\begin{aligned} \hat{B} &= \frac{x \hat{x} + y \hat{y} + z \hat{z}}{\sqrt{x^2 + y^2 + z^2}} \\ \hat{\theta} &= \frac{xz \hat{x} + yz \hat{y} - (x^2 + y^2) \hat{z}}{\sqrt{x^2 + y^2} \sqrt{x^2 + y^2 + z^2}} \\ \hat{\phi} &= \frac{-y \hat{x} + x \hat{y}}{\sqrt{x^2 + y^2}}. \end{aligned} \quad (\text{A20})$$

The Berry phase, given by the integral of the Berry connection along a closed loop  $\mathcal{C}$  in parameter space, can be written as

$$\gamma = \int_{\mathcal{C}} \vec{A}^{(C)} \cdot d\vec{B} = \int_{\mathcal{C}} \vec{A}^{(S)} \cdot d\vec{B}, \quad (\text{A21})$$

where  $d\vec{B} = dx \hat{x} + dy \hat{y} + dz \hat{z}$  in Cartesian coordinates and  $d\vec{B} = dB \hat{B} + B d\theta \hat{\theta} + B \sin \theta d\phi \hat{\phi}$  in spherical coordinates.

The relation  $|\Psi_0(B, \theta, \phi)\rangle = R^\dagger(\phi) |\Psi_0(B, \theta, 0)\rangle$ , where  $R(\phi) = \exp(i\phi \sigma_{\text{tot}}^z / 2)$ , allows us to calculate the Berry connection in spherical coordinates straightforwardly. First, observe that the quantities  $\langle \Psi_0 | \partial_\mu | \Psi_0 \rangle$ , for  $\mu = \{B, \theta, \phi\}$ , must be purely imaginary numbers. This can be seen by differentiating the normalization condition  $\langle \Psi_0 | \Psi_0 \rangle = 1$  with respect to either  $B, \theta$  or  $\phi$ . A gauge choice allows us to choose the eigenstates of the Hamiltonian (A6) to be real at  $\phi = 0$ , and therefore, for any  $B$  and  $\theta$ , writing  $|\Psi_0(B, \theta, \phi)\rangle \equiv |\tilde{\Psi}_0(\phi)\rangle$ , we have

$$\langle \tilde{\Psi}_0(\phi) | \partial_B | \tilde{\Psi}_0(\phi) \rangle = \langle \tilde{\Psi}_0(0) | \partial_B | \tilde{\Psi}_0(0) \rangle = 0. \quad (\text{A22})$$

A similar reasoning holds for  $\langle \Psi_0(B, \theta, \phi) | \partial_\theta | \Psi_0(B, \theta, \phi) \rangle$ . The only non-vanishing component is  $A_\phi$ , which reads

$$\begin{aligned} A_\phi &= i \frac{1}{B \sin \theta} \langle \tilde{\Psi}_0(\phi) | \partial_\phi | \tilde{\Psi}_0(\phi) \rangle \\ &= \frac{1}{B \sin \theta} \langle \tilde{\Psi}_0(0) | i R(\phi) \partial_\phi R^\dagger(\phi) | \tilde{\Psi}_0(0) \rangle, \end{aligned} \quad (\text{A23})$$

and since

$$i R(\phi) \partial_\phi R^\dagger(\phi) = i e^{i\phi \sigma_{\text{tot}}^z / 2} \partial_\phi e^{-i\phi \sigma_{\text{tot}}^z / 2} = \frac{\sigma_{\text{tot}}^z}{2}, \quad (\text{A24})$$

the Berry connection in spherical coordinates is finally given by

$$\begin{aligned} \vec{A}^{(S)}(B, \theta, \phi) &= \frac{1}{B \sin \theta} \langle \tilde{\Psi}_0(0) | \frac{\sigma_{\text{tot}}^z}{2} | \tilde{\Psi}_0(0) \rangle \hat{\phi} \\ &= \frac{1}{B \sin \theta} \frac{\langle \sigma_{\text{tot}}^z \rangle}{2} \hat{\phi}, \end{aligned} \quad (\text{A25})$$

where  $\langle \sigma_{\text{tot}}^z \rangle$  is the ground-state expectation value of the total magnetization in the  $z$ -direction at  $\phi = 0$ . In Cartesian coordinates, we have

$$\vec{A}^{(C)}(x, y, z) = \frac{\langle \sigma_{\text{tot}}^z \rangle}{2} \left( \frac{-y \hat{x} + x \hat{y}}{x^2 + y^2} \right), \quad (\text{A26})$$

with  $\langle \sigma_{\text{tot}}^z \rangle$ , the ground-state expectation value of the total magnetization in the  $z$ -direction given in Cartesian coordinates at  $B_y = 0$ . The Berry curvature  $\vec{F}$  is obtained by taking the curl of the Berry connection.

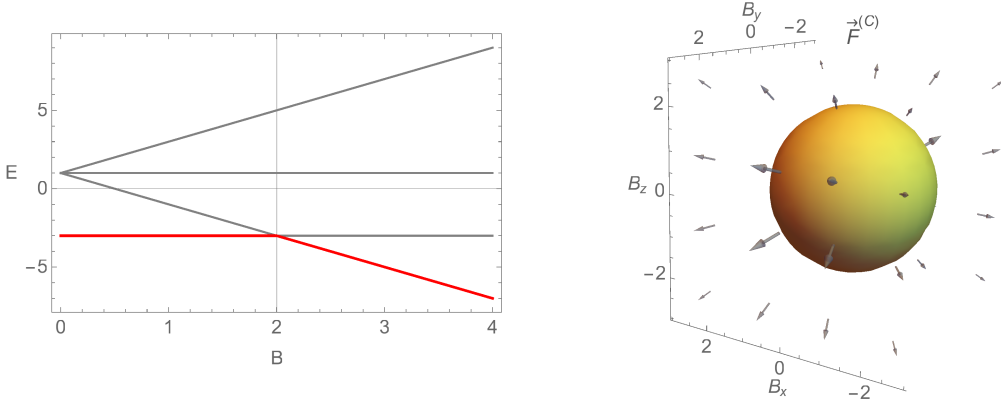


FIG. 3. *Left panel:* The Energy spectrum of the Heisenberg Hamiltonian  $H_{\text{Heis}}$  as a function of  $B$  is depicted. The ground-state energy  $E_0(B)$  is shown by the thick red line. *Right panel:* The Berry curvature in Cartesian coordinates (B9) is plotted in parameter space  $(B_x, B_y, B_z)$ . The sphere of radius  $B = 2$  carries a magnetic charge  $q_m = 2$ , which is uniformly distributed over the surface of this sphere.

### Appendix B: Heisenberg Interaction

In this section, we set  $\gamma_1 = \gamma_2 = g_z = 1$ ,  $g = 2$  and  $B_0 = 0$  in the Hamiltonian (A6) in order to obtain the two-qubit Heisenberg Hamiltonian

$$H_{\text{Heis}} = \vec{B} \cdot (\vec{\sigma}_1 + \vec{\sigma}_2) + \vec{\sigma}_1 \cdot \vec{\sigma}_2. \quad (\text{B1})$$

This Hamiltonian has  $SU(2)$  symmetry, which can be seen immediately using spherical coordinates  $(B, \theta, \phi)$

$$H_{\text{Heis}}(B, \theta, \phi) = B \hat{B}(\theta, \phi) \cdot (\vec{\sigma}_1 + \vec{\sigma}_2) + \vec{\sigma}_1 \cdot \vec{\sigma}_2. \quad (\text{B2})$$

Namely, one observes that

$$D(\hat{B}, \alpha) H_{\text{Heis}} D^\dagger(\hat{B}, \alpha) = H_{\text{Heis}}, \quad (\text{B3})$$

where  $D(\hat{B}, \alpha) = \exp[i\alpha \hat{B} \cdot (\vec{\sigma}_1 + \vec{\sigma}_2)]$  is a generic element of  $SU(2)$  and can be interpreted as a rotation around the axis  $\hat{B}(\theta, \phi)$  by an angle  $\alpha$ . We note that we also have an exchange symmetry between the two qubits  $\vec{\sigma}_1 \leftrightarrow \vec{\sigma}_2$ . As already mentioned previously, we can use the property  $H_{\text{Heis}}(B, \theta, \phi) = R^\dagger(\phi) H_{\text{Heis}}(B, \theta, 0) R(\phi)$  to easily calculate the eigenenergies, eigenstates and thus the Berry connection. The ground-state energy is given by

$$E_0(B) = \begin{cases} -3, & B < 2, \\ 1 - 2B, & B > 2, \end{cases} \quad (\text{B4})$$

and the corresponding ground-state reads

$$|\tilde{\Psi}_0(\phi)\rangle = \begin{cases} \frac{1}{\sqrt{2}}(0, 1, -1, 0)^T, \\ \left( e^{-i\phi} \sin^2 \frac{\theta}{2}, -\frac{\sin \theta}{2}, -\frac{\sin \theta}{2}, e^{i\phi} \cos^2 \frac{\theta}{2} \right)^T \end{cases} \quad (\text{B5})$$

for  $B < 2$  and  $B > 2$ , respectively, where we used the basis  $\{|\uparrow\uparrow\rangle = (1, 0, 0, 0)^T, |\uparrow\downarrow\rangle =$

$(0, 1, 0, 0)^T, |\downarrow\uparrow\rangle = (0, 0, 1, 0)^T, |\downarrow\downarrow\rangle = (0, 0, 0, 1)^T\}$ , since  $\{|\uparrow\rangle = (1, 0)^T, |\downarrow\rangle = (0, 1)^T\}$  are the eigenstates of  $\sigma_z^z$ . We observe that the ground-state degenerates on a sphere of radius  $B = 2$  in the parameter space  $\mathcal{M} \equiv \mathbb{R}^3$  defined in Cartesian coordinates by  $(B_x, B_y, B_z)$ . As illustrated in what follows, this degeneracy surface can be interpreted as a magnetically charged sphere in parameter space which creates an effective magnetic field, the Berry curvature  $\vec{F}$ .

The Berry connection in spherical coordinates can be calculated explicitly, and we find

$$\vec{A}^{(S)}(B, \theta, \phi) = A_\phi \hat{\phi} = \begin{cases} 0, & B < 2, \\ -\frac{1}{B} \cot \theta \hat{\phi} & B > 2. \end{cases} \quad (\text{B6})$$

The Berry curvature, obtained by taking the curl of  $\vec{A}^{(S)}(B, \theta, \phi)$  in spherical coordinates, reads

$$\vec{F}^{(S)}(B, \theta, \phi) = \frac{1}{B \sin \theta} \partial_\theta (A_\phi \sin \theta) \hat{B}, \quad (\text{B7})$$

$$\vec{F}^{(S)}(B, \theta, \phi) = \begin{cases} 0, & B < 2, \\ \frac{1}{2} q_m \frac{1}{B^2} \hat{B}, & B > 2, \end{cases}$$

where  $q_m = 2$  can be interpreted as an effective magnetic charge. The Berry curvature allows us to read the first Chern number, which indeed corresponds to the effective magnetic charge  $q_m$ ,

$$\text{ch}_1 = \frac{1}{2\pi} \iint_{\Sigma} \vec{F}^{(S)} \cdot d\vec{S},$$

$$\text{ch}_1 = \frac{1}{2\pi} \int_0^\pi \int_0^{2\pi} \frac{1}{B^2} B^2 \sin \theta d\theta d\phi = 2 = q_m. \quad (\text{B8})$$

We used the fact that the surface element  $d\vec{S}$  is strictly radial  $d\vec{S} = B^2 \sin \theta d\theta d\phi \hat{B}$ , and choose a spherical Gaussian surface  $\Sigma$  centered at the origin with radius

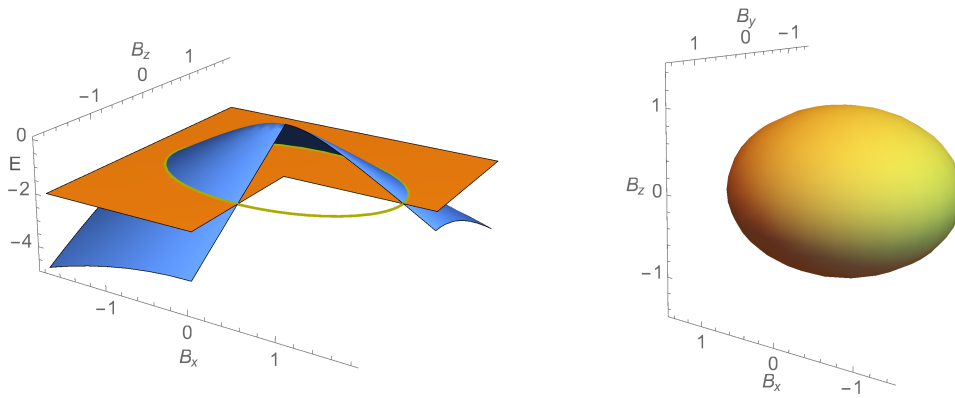


FIG. 4. *Left panel:* The two lowest eigenenergies of  $H_{\text{XXZ}}$  are plotted as a function of  $B_x$  and  $B_z$  for  $g_z = 0.01$  and  $B_y = 0$ . The singlet-state has constant energy given by  $E_{\text{singlet}} = -(2 + g_z)$ , and is shown by the constant (orange) plane, which cuts the (blue) surface corresponding to the eigenenergy of the next lowest eigenstate. The crossing curve, defined by the intersection of these two lowest eigenenergies, is given by an ellipse (yellow). *Right panel:* The locus of the ground-state degeneracy defined by (C3), the surface of an ellipsoid, is plotted in parameter space  $(B_x, B_y, B_z)$ .

$B > 2$  to calculate the above integral. In Fig. 3 we show the spectrum of  $H_{\text{Heis}}$  and the effective magnetic field given by the Berry curvature

$$\vec{F}^{(C)}(B_x, B_y, B_z) = \begin{cases} 0, \\ \frac{1}{2} q m \frac{\vec{B}}{(B_x^2 + B_y^2 + B_z^2)^{3/2}}, \end{cases} \quad (\text{B9})$$

for  $\sqrt{B_x^2 + B_y^2 + B_z^2} < 2$  and  $\sqrt{B_x^2 + B_y^2 + B_z^2} > 2$ , respectively.

### Appendix C: XXZ Interaction

In this section, we choose  $\gamma_1 = \gamma_2 = 1$ ,  $g = 2$ ,  $B_0 = 0$  and  $g_z \neq 1$  in the Hamiltonian (A6), which yields a two-qubit Hamiltonian with XXZ interaction

$$\begin{aligned} H_{\text{XXZ}} &= \vec{B} \cdot (\vec{\sigma}_1 + \vec{\sigma}_2) + (\sigma_1^x \sigma_2^x + \sigma_1^y \sigma_2^y) + g_z \sigma_1^z \sigma_2^z \\ &= \vec{B} \cdot (\vec{\sigma}_1 + \vec{\sigma}_2) + \vec{\sigma}_1 \cdot \vec{\sigma}_2 - (1 - g_z) \sigma_1^z \sigma_2^z. \end{aligned} \quad (\text{C1})$$

This Hamiltonian is no longer  $SU(2)$  symmetric but still has the exchange symmetry between the two qubits. Further, due to the property  $H_{\text{XXZ}}(B, \theta, \phi) = R^\dagger(\phi) H_{\text{XXZ}}(B, \theta, 0) R(\phi)$ , we can set  $B_y = 0$  and using a more appropriate basis given by  $\{|\uparrow\uparrow\rangle, |\downarrow\downarrow\rangle, (|\uparrow\downarrow\rangle + |\downarrow\uparrow\rangle)/\sqrt{2}, (|\uparrow\downarrow\rangle - |\downarrow\uparrow\rangle)/\sqrt{2}\}$ , the Hamiltonian is written as a  $4 \times 4$  matrix,

$$H_{\text{XXZ}} = \begin{pmatrix} 2B_z + g_z & 0 & \sqrt{2} B_x & 0 \\ 0 & -2B_z + g_z & \sqrt{2} B_x & 0 \\ \sqrt{2} B_x & \sqrt{2} B_x & 2 - g_z & 0 \\ 0 & 0 & 0 & -2 - g_z \end{pmatrix}. \quad (\text{C2})$$

One can immediately see that the singlet-state  $(|\uparrow\downarrow\rangle - |\downarrow\uparrow\rangle)/\sqrt{2}$  is an eigenstate with eigenenergy  $E_{\text{singlet}} =$

$-(2 + g_z)$ . More precisely, the singlet-state is the ground-state inside the locus of crossing points given by

$$\frac{B_x^2}{2(1 + g_z)} + \frac{B_y^2}{2(1 + g_z)} + \frac{B_z^2}{(1 + g_z)^2} = 1. \quad (\text{C3})$$

The above expression defines the surface of an ellipsoid in the parameter space  $(B_x, B_y, B_z)$ , and can be obtained by solving the equation for the energy crossing between the singlet-state and the only other state with negative energy for  $B_y = 0$ , applying next the rotation  $R(\phi) = \exp(i\phi \sigma_{\text{tot}}^z / 2)$  to obtain the result (C3) for  $B_y \neq 0$  (see Fig. 4). The ground-state inside the ellipsoid is thus the Bell entangled singlet-state

$$|\Psi_0\rangle = \frac{1}{\sqrt{2}}(|\uparrow\downarrow\rangle - |\downarrow\uparrow\rangle) = \frac{1}{\sqrt{2}}(0, 1, -1, 0)^T, \quad (\text{C4})$$

and hence the Berry connection vanishes inside the ellipsoid, since  $\vec{A}^{(S)} = \frac{1}{B \sin \theta} \langle \sigma_{\text{tot}}^z \rangle \hat{\phi}$ . The Berry connection acquires only a non-zero value outside the ellipsoid, which was calculated numerically using the standard numerical diagonalization techniques. The corresponding Berry curvature and its curl are depicted in Fig. 6.

#### 1. Surface and Charge Density on the Ellipsoid

The magnetic surface charge density  $\sigma_m$  and effective electric surface current  $\vec{K}_e$  associated with the curl of  $\vec{F}$  are calculated in the following by considering the discontinuity in the normal and parallel components of the magnetic field  $\vec{F}$  across the degeneracy surface (the ellipsoid)<sup>25</sup>. The magnetic surface charge density can be calculated from the identity

$$(F_{\text{out}}^\perp - F_{\text{in}}^\perp) = 2\pi\sigma_m, \quad (\text{C5})$$

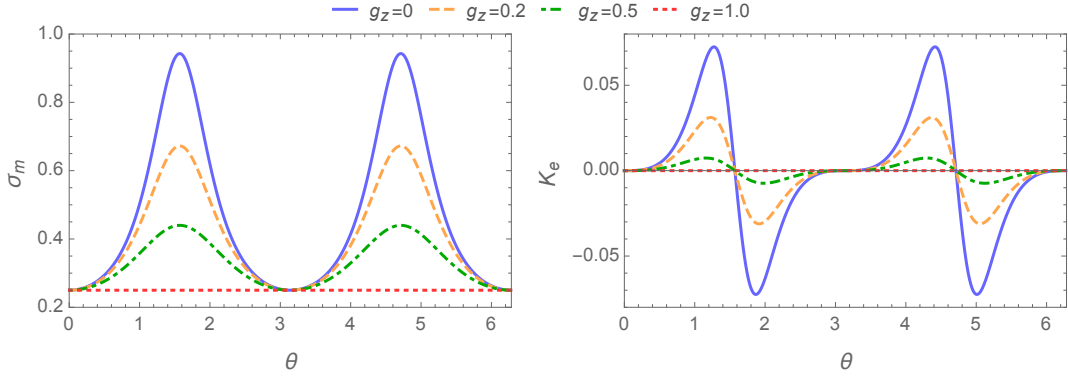


FIG. 5. *Left panel:* The surface charge density  $\sigma_m$  is shown as a function of  $\theta$  for different values of  $g_z$ . Note that we plot  $\theta$  from 0 to  $2\pi$ , which means we go once around the entire ellipsoid. One can see the charge accumulates on the equator as  $g_z$  decreases from 1 to 0. *Right panel:* The surface current density  $K_e$  as a function of  $\theta$  for different  $g_z$  values is depicted.  $K_e$  changes sign at the equator ( $\pi/2$  and  $3\pi/2$ ), indicating the quadrupole configuration pattern of  $\vec{\nabla} \times \vec{F}$ .

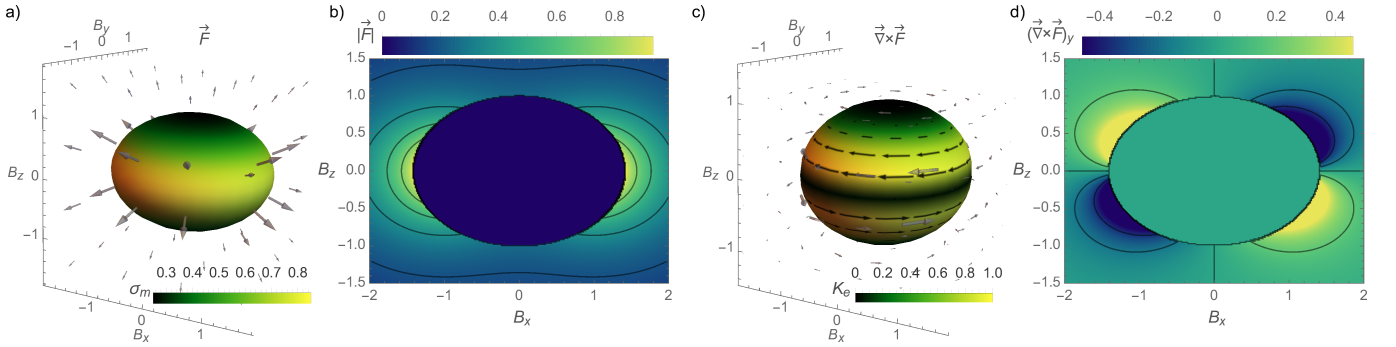


FIG. 6. a) The surface charge density  $\sigma_m$  on the ellipsoid with  $\vec{F}$  for  $g_z = 0$ . b) The corresponding  $|\vec{F}|$  in the  $xz$ -plane. c) The surface electric current density  $K_e$  with  $\vec{\nabla} \times \vec{F}$  for  $g_z = 0$  and in d) we plotted  $(\vec{\nabla} \times \vec{F})_y$  in the  $xz$ -plane.

where  $F_{\text{out}}^\perp$  ( $F_{\text{in}}^\perp$ ) refers to the perpendicular component of  $\vec{F}$  just outside (inside) the charged boundary surface. The total charge  $q_m$  in this example is obtained by  $q_m = \frac{1}{2\pi} \iint_S \sigma_m(\vec{r}) dS$ , where  $dS$  is the differential area element of the ellipsoid surface. Further, the electric surface current can be calculated through

$$\hat{n} \times (\vec{F}_{\text{out}} - \vec{F}_{\text{in}}) = 2\pi \vec{K}_e, \quad (\text{C6})$$

where  $\vec{F}_{\text{out}}$  ( $\vec{F}_{\text{in}}$ ) refers to  $\vec{F}$  just outside (inside) the ellipsoid and  $\hat{n}$  is a unit vector perpendicular to the surface. Both the surface charge density and surface current density are plotted in Fig. 5 versus the polar angle  $\theta$  for different values of  $g_z$ . We note that the property  $H_{\text{XXZ}}(B, \theta, \phi) = R^\dagger(\phi) H_{\text{XXZ}}(B, \theta, 0) R(\phi)$  implies that  $\sigma_m$  and  $\vec{K}_e$  are independent of the azimuthal angle  $\phi$ . In Fig. 6 we plot  $\sigma_m$  and  $K_e$  on the surface of the ellipsoid. The total charge was also computed numerically and found to be  $q_m = +2$  for any value of  $g_z$ , as required from topological considerations ( $\text{ch}_1 = 2$ ).

#### Appendix D: Anisotropic Interaction

In this section, we set  $\gamma_1 = 1 + \alpha$ ,  $\gamma_2 = 1 - \alpha$ ,  $g = 2$ ,  $B_0 = 0$  and  $g_z = 0$ , with  $-1 < \alpha < 1$  in the Hamiltonian (A6), such that we obtain a two-qubit Hamiltonian where the magnetic field  $\vec{B}$  acts anisotropically on each spin

$$H_{\text{ani}} = \vec{B} \cdot [(1 + \alpha) \vec{\sigma}_1 + (1 - \alpha) \vec{\sigma}_2] + \frac{g}{2} (\sigma_1^x \sigma_2^x + \sigma_1^y \sigma_2^y). \quad (\text{D1})$$

Writing this Hamiltonian in spherical coordinates, it can be seen that  $H_{\text{ani}}(B, \theta, \phi) = R^\dagger(\phi) H_{\text{ani}}(B, \theta, 0) R(\phi)$ , still holds and therefore it is sufficient to study the spectrum for  $B_y = 0$ . Let us rewrite  $H_{\text{ani}}$  for  $B_y = 0$  in the basis  $\{|\uparrow\uparrow\rangle, |\uparrow\downarrow\rangle, |\downarrow\uparrow\rangle, |\downarrow\downarrow\rangle\}$ , defining  $\alpha_\pm \equiv (1 \pm \alpha)$  for notational brevity,

$$H_{\text{ani}}(B_x, B_z) = \begin{pmatrix} 2B_z & \alpha_- B_x & \alpha_+ B_x & 0 \\ \alpha_- B_x & 2\alpha B_z & 2 & \alpha_+ B_x \\ \alpha_+ B_x & 2 & -2\alpha B_z & \alpha_- B_x \\ 0 & \alpha_+ B_x & \alpha_- B_x & -2B_z \end{pmatrix}. \quad (\text{D2})$$

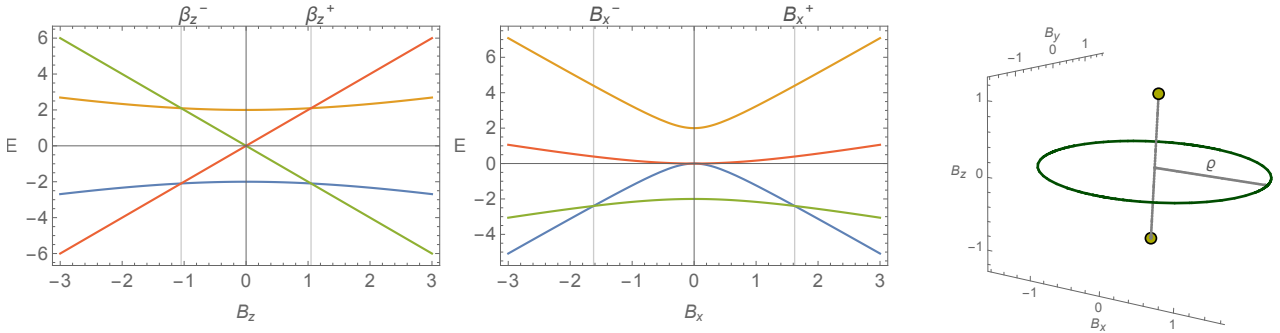


FIG. 7. In the left panel we show a plot of the energy spectrum of  $H_{\text{ani}}(0, 0, B_z)$ , in the middle the eigenenergies of  $H_{\text{ani}}(B_x, 0, 0)$  and on the right panel we depict the ground-state degeneracies in the parameter space  $(B_x, B_y, B_z)$ .

Obviously, for  $B_x = 0$ , the matrix becomes block-diagonal, and the ground-state energy crossings are located at

$$\beta_z^{(\pm)} = \pm \frac{1}{\sqrt{(1 - \alpha^2)}}. \quad (\text{D3})$$

In the case of  $B_z = 0$ , the Hamiltonian  $H_{\text{ani}}(B_x, 0, 0)$  commutes with  $\sigma_1^x \sigma_2^x$  and therefore they have a common basis of eigenvectors given by  $\{(-|\uparrow\uparrow\rangle + |\downarrow\downarrow\rangle)/\sqrt{2}, (-|\uparrow\downarrow\rangle + |\downarrow\uparrow\rangle)/\sqrt{2}, (|\uparrow\uparrow\rangle + |\downarrow\downarrow\rangle)/\sqrt{2}, (|\uparrow\downarrow\rangle + |\downarrow\uparrow\rangle)/\sqrt{2}\}$ . With respect to this basis,  $H_{\text{ani}}(B_x, 0, 0)$  is block-diagonal,

$$H_{\text{ani}}(B_x, 0, 0) = \begin{pmatrix} 0 & -2\alpha B_x & 0 & 0 \\ -2\alpha B_x & -2 & 0 & 0 \\ 0 & 0 & 0 & 2B_x \\ 0 & 0 & 2B_x & 2 \end{pmatrix}, \quad (\text{D4})$$

where the corresponding eigenenergies can easily be calculated,

$$E_1 = 1 - \sqrt{1 + 4B_x^2}, \quad E_2 = -1 - \sqrt{1 + 4\alpha^2 B_x^2}, \\ E_3 = -1 + \sqrt{1 + 4\alpha^2 B_x^2}, \quad E_4 = 1 + \sqrt{1 + 4B_x^2}, \quad (\text{D5})$$

and it can be seen that the ground-state energy degenerates ( $E_1 = E_2$ ) at  $B_x^{(\pm)} = \pm \sqrt{2(1 + \alpha^2)}/(1 - \alpha^2)$ . The azimuthal invariance of the eigenenergies (the property  $H_{\text{ani}}(B, \theta, \phi) = R^\dagger(\phi)H_{\text{ani}}(B, \theta, 0)R(\phi)$ ), implies that these two points in the  $xz$ -plane actually correspond to a ring centered at the origin in the  $xy$ -plane, with radius

$$\varrho = \frac{\sqrt{2(1 + \alpha^2)}}{(1 - \alpha^2)}. \quad (\text{D6})$$

In Fig. 7 we plot the spectrum of the two-qubit Hamiltonian with an anisotropic magnetic field and the ground-state degeneracies in parameter space  $(B_x, B_y, B_z)$ , given by a ring in the  $xy$ -plane and two points on the  $z$ -axis.

Finally, we note that the ring has no charge, which can be seen by calculating the first Chern number numerically,  $\text{ch}_1(\text{ring}) = 0$ . On the contrary, the two point

charges on the  $z$ -axis carry each a charge of  $+1$ . This was also confirmed by a numerical evaluation of the first Chern number. Energy-level crossings that yield a trivial Berry phase when encircled, and therefore have an associated zero Chern number, are known as Renner-Teller level touchings<sup>22</sup>. The energy level touching can be observed by fixing  $B_x = \varrho$  and varying  $B_z$  (see Fig. 8).

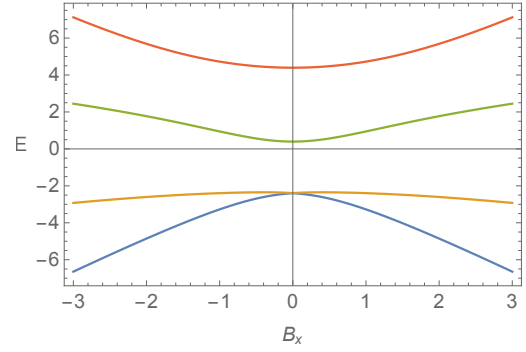


FIG. 8. Renner-Teller level touching for  $B_x = \varrho$  and changing  $B_z$ , i.e., vertically crossing the ring.

## Appendix E: Broken Exchange Symmetry

In this section we calculate the Berry connection  $\vec{A}$  (vector potential), Berry curvature  $\vec{F}$  (magnetic field) and the curl of the Berry curvature  $\nabla \times \vec{F}$  (current) using a degenerate perturbation theory for the interacting two-qubit system with broken exchange symmetry. First, we derive the location of the ground-state degeneracies (level crossings) in the parameter space. Next, we compute the ground-state of the system up to second-order using a degenerate perturbation theory. The resulting ground-state allows us then to calculate the Berry connection, Berry curvature and the curl of the Berry curvature in the vicinity of the effective magnetic monopole charges (ground-state degeneracies).

### 1. Location of the magnetic monopoles

The Hamiltonian for two interacting qubits with a broken exchange symmetry is given by

$$H_{\text{BES}} = \vec{B} \cdot (\vec{\sigma}_1 + \vec{\sigma}_2) + \frac{g}{2}(\sigma_1^x \sigma_2^x + \sigma_1^y \sigma_2^y) + B_0 \sigma_1^z, \quad (\text{E1})$$

which can be obtained by setting  $\gamma_1 = \gamma_2 = 1$  and  $g_z = 0$  in the Hamiltonian (A6). The ground-state degeneracies are restricted to the  $B_z$  axis, since the eigenenergies of the Hamiltonian (E1) have an azimuthal symmetry, and since the Hamiltonian (E1) itself has no more symmetries. The positions of the ground-state degeneracies in parameter space can therefore be determined by diagonalizing the Hamiltonian (E1) for  $B_x = B_y = 0$ . In the basis  $\{|\uparrow\uparrow\rangle, |\uparrow\downarrow\rangle, |\downarrow\uparrow\rangle, |\downarrow\downarrow\rangle\}$  the Hamiltonian becomes block-diagonal

$$H_{\text{BES}}(0, 0, B_z) = \begin{pmatrix} B_0 + 2B_z & 0 & 0 & 0 \\ 0 & B_0 & g & 0 \\ 0 & g & -B_0 & 0 \\ 0 & 0 & 0 & -B_0 - 2B_z \end{pmatrix}, \quad (\text{E2})$$

and thus the corresponding eigenenergies  $E_n$  and eigenstates  $|\psi_n\rangle$ , with  $n = 1, 2, 3, 4$ , are given by

$$\begin{aligned} E_1 &= -B_0 - 2B_z, & |\psi_1\rangle &= (0, 0, 0, 1)^T, \\ E_2 &= -\delta, & |\psi_2\rangle &= \frac{1}{\sqrt{(B_z^+)^2 + (\frac{g}{2})^2}}(0, -B_z^+, \frac{g}{2}, 0)^T, \\ E_3 &= B_0 + 2B_z, & |\psi_3\rangle &= (1, 0, 0, 0)^T, \\ E_4 &= \delta, & |\psi_4\rangle &= \frac{1}{\sqrt{(B_z^-)^2 + (\frac{g}{2})^2}}(0, -B_z^-, \frac{g}{2}, 0)^T, \end{aligned} \quad (\text{E3})$$

where we defined

$$\begin{aligned} \delta &\equiv \sqrt{B_0^2 + g^2}, \\ B_z^+ &\equiv \frac{1}{2}(-B_0 + \delta), & B_z^- &\equiv \frac{1}{2}(-B_0 - \delta). \end{aligned} \quad (\text{E4})$$

In Fig. 9, we plot the eigenenergies  $E_n$  as a function of  $B_z$  for  $B_x = B_y = 0$  with fixed  $B_0$  and  $g$ . It shows that the ground-state energy-level crosses with the excited energy-levels at  $B_z = B_z^-$  and  $B_z = B_z^+$ . These degeneracies act as magnetic monopoles in parameter space. The ground-state energy of the system as a function of  $B_z$  for  $B_x = B_y = 0$  can be written as

$$E_0(B_z) = \begin{cases} -B_0 - 2B_z, & B_z \geq B_z^+, \\ -\delta, & B_z^- \leq B_z \leq B_z^+, \\ B_0 + 2B_z, & B_z \leq B_z^- \end{cases} \quad (\text{E5})$$

and the corresponding ground-state reads

$$|\Psi_0(B_z)\rangle = \begin{cases} (0, 0, 0, 1)^T, & B_z \geq B_z^+, \\ \frac{(0, -B_z^+, g/2, 0)^T}{\sqrt{(B_z^+)^2 + (g/2)^2}}, & B_z^- \leq B_z \leq B_z^+, \\ (1, 0, 0, 0)^T, & B_z \leq B_z^-. \end{cases} \quad (\text{E6})$$

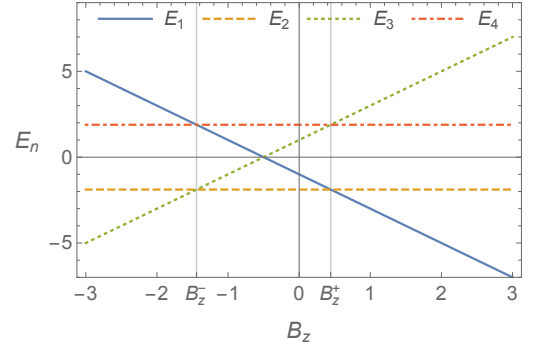


FIG. 9. Eigenenergies as a function of  $B_z$  for  $B_x = B_y = 0$  and fixed  $B_0$  and  $g$ . The degeneracies of the ground-state occur at  $B_z = B_z^-$  and  $B_z = B_z^+$ .

### Appendix F: Degenerate perturbation theory: Coordinate system centered at monopoles

In what follows we use a degenerate perturbation theory to calculate the ground-state of our two qubit system close to the degeneracies at  $B_z^+$  and  $B_z^-$ . We will present only the results for small deviations around the degeneracy  $B_z^+$ ; the results around  $B_z^-$  are obtained in a similar way. Let us consider the location of the degeneracy, given vectorially by  $\vec{B}' = (0, 0, B_z^+)^T$ , as the origin of a new coordinate system. With respect to this new coordinate system, a point in parameter space  $(B_x, B_y, B_z)$  is indicated by the vector  $d\vec{B} = (dB_x, dB_y, dB_z)^T$  and it is related to the original coordinate system by  $d\vec{B} = \vec{B} - \vec{B}'$ , which yields the following relations between the two coordinate systems

$$\vec{B} = \begin{pmatrix} B_x \\ B_y \\ B_z \end{pmatrix} = \vec{B}' + d\vec{B} = \begin{pmatrix} dB_x \\ dB_y \\ dB_z + B_z^+ \end{pmatrix}. \quad (\text{F1})$$

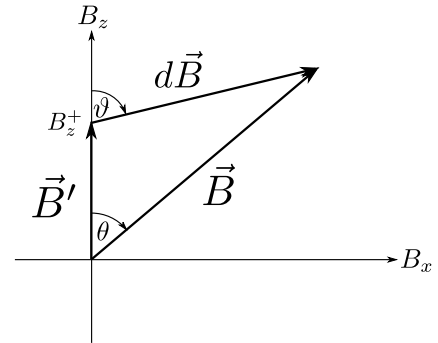


FIG. 10. The two different coordinate systems:  $\vec{B}$  and  $d\vec{B}$ .

The Hamiltonian (E1) in the new coordinates reads

$$H_{\text{BES}} = dB_x(\sigma_1^x + \sigma_2^x) + dB_y(\sigma_1^y + \sigma_2^y) + dB_z(\sigma_1^z + \sigma_2^z) + B_z^+(\sigma_1^z + \sigma_2^z) + \frac{g}{2}(\sigma_1^x\sigma_2^x + \sigma_1^y\sigma_2^y) + B_0\sigma_1^z. \quad (\text{F2})$$

We treat the deviation from the monopole (degeneracy) as a small perturbation, i.e.,  $|d\vec{B}| \ll 1$ . It is therefore useful to express (F1) in spherical coordinates

$$d\vec{B} = \begin{pmatrix} dB \sin \vartheta \cos \phi \\ dB \sin \vartheta \sin \phi \\ dB \cos \vartheta \end{pmatrix} = \vec{B} - \vec{B}' = \begin{pmatrix} B \sin \theta \cos \phi \\ B \sin \theta \sin \phi \\ B \cos \theta - B_z^+ \end{pmatrix}, \quad (\text{F3})$$

which yields the relations

$$dB \sin \vartheta = B \sin \theta, \quad dB \cos \vartheta = B \cos \theta - B_z^+. \quad (\text{F4})$$

Let us focus on the  $xz$ -plane defined by  $B_y = 0$ , or in spherical coordinates, by  $\phi = 0$ . Such choice implies  $dB_y = 0$ , and thus we have

$$H_{\text{BES}} = dB_x(\sigma_1^x + \sigma_2^x) + dB_z(\sigma_1^z + \sigma_2^z) + B_z^+(\sigma_1^z + \sigma_2^z) + \frac{g}{2}(\sigma_1^x\sigma_2^x + \sigma_1^y\sigma_2^y) + B_0\sigma_1^z = H_0 + dB H' \quad (\text{F5})$$

where

$$H_0 = B_z^+(\sigma_1^z + \sigma_2^z) + \frac{g}{2}(\sigma_1^x\sigma_2^x + \sigma_1^y\sigma_2^y) + B_0\sigma_1^z, \quad H' = \sin \vartheta (\sigma_1^x + \sigma_2^x) + \cos \vartheta (\sigma_1^z + \sigma_2^z). \quad (\text{F6})$$

### 1. Degenerate perturbation theory: ground-state calculation

First, we calculate the eigenvalues and eigenstates of  $H_0$ . The eigenenergies are given by

$$E_1^{(0)} = -\sqrt{B_0^2 + g^2}, \quad E_2^{(0)} = -\sqrt{B_0^2 + g^2}, \quad E_3^{(0)} = \sqrt{B_0^2 + g^2}, \quad E_4^{(0)} = \sqrt{B_0^2 + g^2}, \quad (\text{F7})$$

and the corresponding eigenstates read

$$\begin{aligned} |\Psi_1^{(0)}\rangle &= (0, 0, 0, 1)^T, \\ |\Psi_2^{(0)}\rangle &= \left(0, -\frac{B_z^+}{\sqrt{(B_z^+)^2 + (g/2)^2}}, \frac{(g/2)}{\sqrt{(B_z^+)^2 + (g/2)^2}}, 0\right)^T, \\ |\Psi_3^{(0)}\rangle &= \left(0, -\frac{B_z^-}{\sqrt{(B_z^-)^2 + (g/2)^2}}, \frac{(g/2)}{\sqrt{(B_z^-)^2 + (g/2)^2}}, 0\right)^T, \\ |\Psi_4^{(0)}\rangle &= (1, 0, 0, 0)^T. \end{aligned} \quad (\text{F8})$$

The location of the energy level crossings of the ground-state and the first excited state on the  $z$ -axis appear at

$$B_z^+ = \frac{1}{2}(-B_0 + \sqrt{B_0^2 + g^2}), \quad B_z^- = \frac{1}{2}(-B_0 - \sqrt{B_0^2 + g^2}). \quad (\text{F9})$$

We note the following useful identities

$$B_z^+ + B_z^- = -B_0, \quad B_z^+ - B_z^- = \sqrt{B_0^2 + g^2} \equiv \delta. \quad (\text{F10})$$

Let us also introduce the following notations,

$$\begin{aligned} \delta &\equiv \sqrt{B_0^2 + g^2}, \quad \beta^2 \equiv \frac{g}{\delta}, \\ \Delta &\equiv \frac{B_z^+ - \frac{g}{2}}{\sqrt{(B_z^+)^2 + (g/2)^2}}, \quad \eta \equiv \frac{(B_z^-) - \frac{g}{2}}{\sqrt{(B_z^-)^2 + (g/2)^2}}. \end{aligned} \quad (\text{F11})$$

The unperturbed eigenstates  $\{|\Psi_1^{(0)}\rangle, |\Psi_2^{(0)}\rangle\}$  and  $\{|\Psi_3^{(0)}\rangle, |\Psi_4^{(0)}\rangle\}$  are degenerate, therefore one needs to use a degenerate perturbation theory to compute the first-order corrections. To this end, we write the matrix

$$\begin{aligned} W &= \begin{pmatrix} \langle \Psi_1^{(0)} | H' | \Psi_1^{(0)} \rangle & \langle \Psi_1^{(0)} | H' | \Psi_2^{(0)} \rangle \\ \langle \Psi_2^{(0)} | H' | \Psi_1^{(0)} \rangle & \langle \Psi_2^{(0)} | H' | \Psi_2^{(0)} \rangle \end{pmatrix} \\ &= \begin{pmatrix} -2 \cos \vartheta & -\frac{B_z^+ - g/2}{\sqrt{(B_z^+)^2 + (g/2)^2}} \sin \vartheta \\ -\frac{B_z^+ - g/2}{\sqrt{(B_z^+)^2 + (g/2)^2}} \sin \vartheta & 0 \end{pmatrix} \\ &= \begin{pmatrix} -2 \cos \vartheta & -\Delta \sin \vartheta \\ -\Delta \sin \vartheta & 0 \end{pmatrix}. \end{aligned} \quad (\text{F12})$$

The matrix  $W$  has eigenvalues

$$\begin{aligned} E_{\pm}^{(1)} &= -\cos \vartheta \pm \sqrt{\cos^2 \vartheta + \Delta^2 \sin^2 \vartheta} \\ &= -\cos \vartheta \pm \sqrt{1 - \beta^2 \sin^2 \vartheta}, \end{aligned} \quad (\text{F13})$$

where we used the identities

$$\begin{aligned} \Delta^2 &= \frac{(B_z^+ - g/2)^2}{(B_z^+)^2 + (g/2)^2} = 1 - \frac{2B_z^+(g/2)}{(B_z^+)^2 + (g/2)^2} \\ \Delta^2 &\equiv 1 - \frac{g}{\delta} \equiv 1 - \beta^2. \end{aligned} \quad (\text{F14})$$

The eigenvalues  $E_{\pm}^{(1)}$  of the matrix  $W$  give the first-order correction to the two lowest eigenenergies, namely  $E_{1,2} = E_1^{(0)} + dB E_{\pm}^{(1)}$ . The eigenvectors of  $W$  are written as  $|w_{1,2}\rangle$  and read

$$\begin{aligned} |w_1\rangle &= \begin{pmatrix} a_1 \\ b_1 \end{pmatrix} = \begin{pmatrix} \frac{E_-^{(1)}}{\sqrt{(E_-^{(1)})^2 + \Delta^2 \sin^2 \vartheta}} \\ -\frac{\Delta \sin \vartheta}{\sqrt{(E_-^{(1)})^2 + \Delta^2 \sin^2 \vartheta}} \end{pmatrix}, \\ |w_2\rangle &= \begin{pmatrix} \frac{E_+^{(1)}}{\sqrt{(E_+^{(1)})^2 + \Delta^2 \sin^2 \vartheta}} \\ -\frac{\Delta \sin \vartheta}{\sqrt{(E_+^{(1)})^2 + \Delta^2 \sin^2 \vartheta}} \end{pmatrix}. \end{aligned} \quad (\text{F15})$$

The ‘‘good’’ linear combination for the ground-state at zeroth-order is therefore given by

$$\begin{aligned}
|\Psi_0^{(0)}\rangle &= a_1|\Psi_1^{(0)}\rangle + b_1|\Psi_2^{(0)}\rangle \\
&= \frac{E_-^{(1)}}{\sqrt{(E_-^{(1)})^2 + \Delta^2 \sin^2 \vartheta}} (0, 0, 0, 1)^T + \left( \frac{-\Delta \sin \vartheta}{\sqrt{(E_+^{(1)})^2 + \Delta^2 \sin^2 \vartheta}} \right) \left( 0, \frac{-B_z^+}{\sqrt{(B_z^+)^2 + (\frac{g}{2})^2}}, \frac{(\frac{g}{2})}{\sqrt{(B_z^+)^2 + (\frac{g}{2})^2}}, 0 \right)^T \\
&= \frac{1}{\sqrt{(E_-^{(1)})^2 + \Delta^2 \sin^2 \vartheta}} \left( 0, \frac{B_z^+ \Delta \sin \vartheta}{\sqrt{(B_z^+)^2 + (\frac{g}{2})^2}}, \frac{-(\frac{g}{2}) \Delta \sin \vartheta}{\sqrt{(B_z^+)^2 + (\frac{g}{2})^2}}, E_-^{(1)} \right)^T. \tag{F16}
\end{aligned}$$

---

The first-order correction to the ground-state is

---

$$|\Psi_0^{(1)}\rangle = \sum_{n \neq \{1,2\}} \frac{\langle \Psi_n^{(0)} | H' | \Psi_0^{(0)} \rangle}{(E_1^{(0)} - E_n^{(0)})} |\Psi_n^{(0)}\rangle = -\frac{1}{2\delta} \frac{1}{\sqrt{(E_-^{(1)})^2 + \Delta^2 \sin^2 \vartheta}} \begin{pmatrix} \Delta^2 \sin^2 \vartheta \\ \frac{B_z^-}{B_z^- - \frac{g}{2}} \eta^2 E_-^{(1)} \sin \vartheta \\ -\frac{\frac{g}{2}}{B_z^- - \frac{g}{2}} \eta^2 E_-^{(1)} \sin \vartheta \\ 0 \end{pmatrix}. \tag{F17}$$

---

The second-order correction to the ground-state is given by

---

$$\begin{aligned}
|\Psi_0^{(2)}\rangle &= \sum_{k \neq \{1,2\}} \sum_{l \neq \{1,2\}} \frac{\langle \Psi_k^{(0)} | H' | \Psi_l^{(0)} \rangle \langle \Psi_l^{(0)} | H' | \Psi_0^{(0)} \rangle}{(E_1^{(0)} - E_k^{(0)})(E_1^{(0)} - E_l^{(0)})} |\Psi_k^{(0)}\rangle - \frac{1}{2} |\Psi_0^{(0)}\rangle \sum_{k \neq \{1,2\}} \frac{\langle \Psi_0^{(0)} | H' | \Psi_k^{(0)} \rangle \langle \Psi_k^{(0)} | H' | \Psi_0^{(0)} \rangle}{(E_1^{(0)} - E_k^{(0)})^2} + \\
&\quad - \sum_{k \neq \{1,2\}} \frac{\langle \Psi_0^{(0)} | H' | \Psi_0^{(0)} \rangle \langle \Psi_k^{(0)} | H' | \Psi_0^{(0)} \rangle}{(E_1^{(0)} - E_k^{(0)})^2} |\Psi_k^{(0)}\rangle \tag{F18} \\
&= \frac{1}{4\delta^2} \frac{\Delta^2 \sin^2 \vartheta}{\sqrt{(E_-^{(1)})^2 + \Delta^2 \sin^2 \vartheta}} \begin{pmatrix} \frac{\eta^2}{\Delta^2} E_-^{(1)} + 2 \cos \vartheta \\ \frac{B_z^-}{B_z^- - \frac{g}{2}} \eta^2 \sin \vartheta \\ -\frac{\frac{g}{2}}{B_z^- - \frac{g}{2}} \eta^2 \sin \vartheta \\ 0 \end{pmatrix} + \\
&\quad - \frac{1}{8\delta^2} \frac{\Delta^2 \sin^2 \vartheta}{\sqrt{(E_-^{(1)})^2 + \Delta^2 \sin^2 \vartheta}} \frac{(\frac{\eta^2}{\Delta^2} (E_-^{(1)})^2 + \Delta^2 \sin^2 \vartheta)}{(E_-^{(1)})^2 + \Delta^2 \sin^2 \vartheta} \begin{pmatrix} 0 \\ \frac{B_z^+}{B_z^+ - \frac{g}{2}} \Delta^2 \sin \vartheta \\ -\frac{\frac{g}{2}}{B_z^+ - \frac{g}{2}} \Delta^2 \sin \vartheta \\ E_-^{(1)} \end{pmatrix} + \\
&\quad + \frac{1}{2\delta^2} \frac{E_-^{(1)} \sin \vartheta}{\sqrt{(E_-^{(1)})^2 + \Delta^2 \sin^2 \vartheta}} \frac{(E_-^{(1)} \cos \vartheta - \Delta^2 \sin^2 \vartheta)}{(E_-^{(1)})^2 + \Delta^2 \sin^2 \vartheta} \begin{pmatrix} \Delta^2 \sin \vartheta \\ \frac{B_z^-}{B_z^- - \frac{g}{2}} \eta^2 E_-^{(1)} \\ -\frac{\frac{g}{2}}{B_z^- - \frac{g}{2}} \eta^2 E_-^{(1)} \\ 0 \end{pmatrix}. \tag{F19}
\end{aligned}$$

The ground-state can then be expressed up to second-order by

$$|\Psi_0(dB, \vartheta, 0)\rangle = |\Psi_0^{(0)}\rangle + dB |\Psi_0^{(1)}\rangle + dB^2 |\Psi_0^{(2)}\rangle, \tag{F20}$$

and the dependence on the azimuth angle  $\phi$  is obtained through the following rotation

$$|\Psi_0(dB, \vartheta, \phi)\rangle = R^\dagger(\phi) |\Psi_0(dB, \vartheta, 0)\rangle, \tag{F21}$$

where  $R(\phi) = \exp(i\phi(\hat{\sigma}_1^z + \hat{\sigma}_2^z)/2)$ .

## 2. Berry connection – Effective magnetic vector potential

We are now able to calculate the Berry connection in spherical coordinates  $\vec{A}_+^{(S)}(dB, \vartheta, \phi)$ , where the + sign

$$\begin{aligned}
A_{\phi,+} &= i \frac{1}{dB \sin \vartheta} \langle \Psi_0(dB, \vartheta, \phi) | \partial_\phi | \Psi_0(dB, \vartheta, \phi) \rangle \\
&= \frac{1}{dB \sin \vartheta} \langle \Psi_0(dB, \vartheta, 0) | \frac{1}{2} (\hat{\sigma}_1^z + \hat{\sigma}_2^z) | \Psi_0(dB, \vartheta, 0) \rangle \\
&= \frac{1}{dB \sin \vartheta} \left[ \langle \Psi_0^{(0)} | \frac{1}{2} (\hat{\sigma}_1^z + \hat{\sigma}_2^z) | \Psi_0^{(0)} \rangle + 2 dB \langle \Psi_0^{(0)} | \frac{1}{2} (\hat{\sigma}_1^z + \hat{\sigma}_2^z) | \Psi_0^{(1)} \rangle + \right. \\
&\quad \left. + dB^2 \left( 2 \langle \Psi_0^{(0)} | \frac{1}{2} (\hat{\sigma}_1^z + \hat{\sigma}_2^z) | \Psi_0^{(2)} \rangle + \langle \Psi_0^{(1)} | \frac{1}{2} (\hat{\sigma}_1^z + \hat{\sigma}_2^z) | \Psi_0^{(1)} \rangle \right) + \dots \right] \\
&= \frac{1}{dB \sin \vartheta} \left[ - \frac{(E_-^{(1)})^2}{(E_-^{(1)})^2 + \Delta^2 \sin^2 \vartheta} + dB^2 \frac{1}{4 \delta^2} \frac{\Delta^4 \sin^4 \vartheta}{(E_-^{(1)})^2 + \Delta^2 \sin^2 \vartheta} + \right. \\
&\quad \left. + dB^2 \frac{1}{4 \delta^2} \left( \frac{\eta^2}{\Delta^2} (E_-^{(1)})^2 + \Delta^2 \sin^2 \vartheta \right) \frac{(E_-^{(1)})^2}{(E_-^{(1)})^2 + \Delta^2 \sin^2 \vartheta} \frac{\Delta^2 \sin^2 \vartheta}{(E_-^{(1)})^2 + \Delta^2 \sin^2 \vartheta} + \dots \right] \\
&= \frac{1}{dB \sin \vartheta} \left[ - \frac{1}{2} \left( 1 + \frac{\cos \vartheta}{\sqrt{1 - \beta^2 \sin^2 \vartheta}} \right) + dB^2 \frac{1}{8 \delta^2} \left( 1 - \frac{\cos \vartheta}{\sqrt{1 - \beta^2 \sin^2 \vartheta}} \right) (1 - \beta^2) \sin^2 \vartheta + \right. \\
&\quad \left. + dB^2 \frac{1}{8 \delta^2} \sin^2 \vartheta \left( 1 + \frac{(1 + \beta^2) \cos \vartheta}{\sqrt{1 - \beta^2 \sin^2 \vartheta}} + \frac{\beta^2 \cos^2 \vartheta}{1 - \beta^2 \sin^2 \vartheta} \right) + \dots \right] \\
&\approx \frac{1}{dB \sin \vartheta} \left[ - \frac{1}{2} \left( 1 + \frac{\cos \vartheta}{\sqrt{1 - \beta^2 \sin^2 \vartheta}} \right) + dB^2 \frac{1}{8 \delta^2} \sin^2 \vartheta \left( 2 - \beta^2 + \frac{2\beta^2 \cos \vartheta}{\sqrt{1 - \beta^2 \sin^2 \vartheta}} + \frac{\beta^2 \cos^2 \vartheta}{1 - \beta^2 \sin^2 \vartheta} \right) \right], \quad (\text{F23})
\end{aligned}$$

where

$$\beta^2 = \frac{g}{\delta} = \frac{g}{\sqrt{B_0^2 + g^2}}, \quad \frac{\eta^2}{\Delta^2} = \frac{1 + \beta^2}{1 - \beta^2}. \quad (\text{F24})$$

$$A_{\phi,+} \approx \frac{1}{dB \sin \vartheta} \left[ - \frac{1}{2} \left( 1 + \frac{\cos \vartheta}{\sqrt{1 - \beta^2 \sin^2 \vartheta}} \right) + dB^2 \frac{1}{8 \delta^2} \sin^2 \vartheta \left( 2 - \beta^2 + \frac{2\beta^2 \cos \vartheta}{\sqrt{1 - \beta^2 \sin^2 \vartheta}} + \frac{\beta^2 \cos^2 \vartheta}{1 - \beta^2 \sin^2 \vartheta} \right) \right], \quad (\text{F25})$$

and keeping only the leading order term for  $A_{\phi,+}$  we have

$$A_{\phi,+} \approx - \frac{1}{2} \frac{1}{dB \sin \vartheta} \left( 1 + \frac{\cos \vartheta}{\sqrt{1 - \beta^2 \sin^2 \vartheta}} \right). \quad (\text{F26})$$

indicates that we are considering small radial deviations  $dB$  close to the degeneracy located at  $B_z^+$ . The operator  $\vec{\nabla}$  in spherical coordinates  $(dB, \vartheta, \phi)$  is given by

$$\vec{\nabla} = \left( \frac{\partial}{\partial(dB)}, \frac{1}{dB} \frac{\partial}{\partial \vartheta}, \frac{1}{dB \sin \vartheta} \frac{\partial}{\partial \phi} \right)^T, \quad (\text{F22})$$

therefore the only non zero component of the Berry connection is  $A_{\phi,+}$  and reads

In summary, one can write the Berry connection (vector potential) in spherical coordinates  $\vec{A}_+^{(S)}(dB, \vartheta, \phi) = A_{\phi,+} \hat{\phi}$ , with

## 3. Berry curvature – Effective magnetic field

The Berry curvature  $\vec{F}^{(S)}(dB, \vartheta, \phi)$  is obtained by taking the curl of (F26). The curl operator in spherical co-

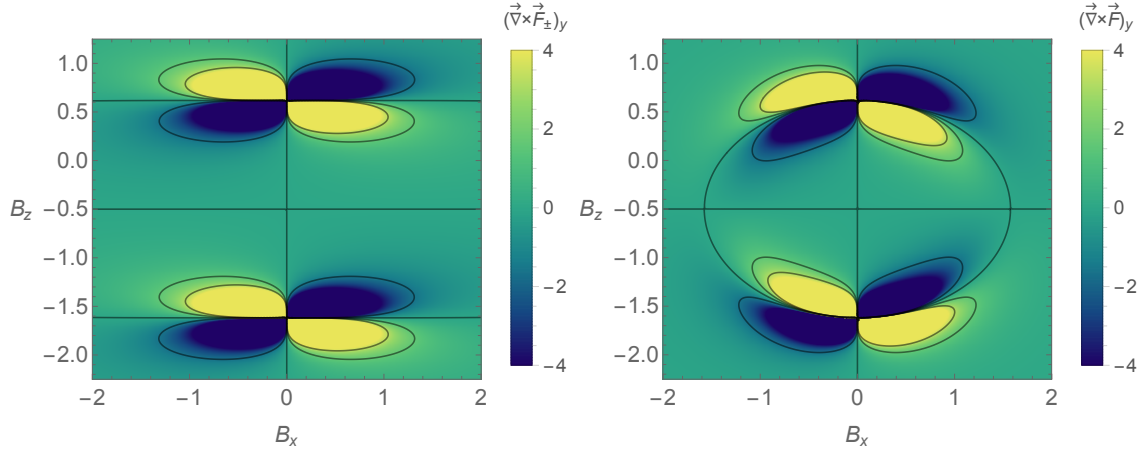


FIG. 11. A density plot of the  $y$  component of  $\vec{\nabla} \times \vec{F}$  in Cartesian coordinates as a function of  $B_x$  and  $B_z$  is shown for  $B_y = 0$ ,  $g = 2$  and  $B_0 = 1$ . The curl of the Berry curvature has only a  $y$  component in the plane defined by  $B_y = 0$ . Negative values indicate that the vectors point perpendicularly out of the plane and positive values indicate the vectors point perpendicularly into the plane. On the left panel we show the curl of the Berry curvature obtained by perturbation theory and on the right obtained by exact diagonalization.

ordinates  $(dB, \vartheta, \phi)$  reads

$$\begin{aligned} \vec{F}^{(S)}(dB, \vartheta, \phi) &= \vec{\nabla} \times \vec{A}^{(S)}(dB, \vartheta, \phi) = \\ &= \frac{1}{dB \sin \vartheta} (\partial_{\vartheta} (A_{\phi} \sin \vartheta) - \partial_{\phi} A_{\vartheta}) d\hat{B} + \frac{1}{dB} \left( \frac{1}{\sin \vartheta} \partial_{\phi} A_{dB} - \partial_{dB} (dBA_{\phi}) \right) \hat{\vartheta} + \frac{1}{dB} (\partial_{dB} (dBA_{\vartheta}) - \partial_{\vartheta} A_{dB}) \hat{\phi}, \end{aligned} \quad (\text{F27})$$

where  $\vec{A}^{(S)}(dB, \vartheta, \phi) = A_{dB} d\hat{B} + A_{\vartheta} \hat{\vartheta} + A_{\phi} \hat{\phi}$ . The only non vanishing component of  $\vec{A}^{(S)}(dB, \vartheta, \phi)$  is  $A_{\phi,+}$  and hence in the leading order of  $dB$  we find

$$\begin{aligned} \vec{F}_+^{(S)}(dB, \vartheta, \phi) &= \vec{\nabla} \times \vec{A}_+^{(S)}(dB, \vartheta, \phi) \\ &\approx \frac{1}{2} \frac{1}{\gamma^2 (1 - \beta^2 \sin^2 \vartheta)^{3/2}} \frac{1}{dB^2} d\hat{B}, \end{aligned} \quad (\text{F28})$$

where we introduced  $\gamma \equiv 1/\sqrt{1 - \beta^2}$ .

#### 4. Curl of Berry curvature

Finally, the curl of the Berry curvature to the leading order in  $dB$  near the monopole  $B_z^+$  can be calculated,

and reads

$$\vec{\nabla} \times \vec{F}_+^{(S)}(dB, \vartheta, \phi) \approx -\frac{3}{4} \frac{\beta^2 \sin 2\vartheta}{\gamma^2 (1 - \beta^2 \sin^2 \vartheta)^{5/2}} \frac{1}{dB^3} \hat{\phi}. \quad (\text{F29})$$

Following exactly the same procedure described above, but applied to the degeneracy located at  $B_z^-$ , one finds that the leading order of  $A_{\phi,-}$  is given by

$$A_{\phi,-} \approx \frac{1}{2} \frac{1}{dB \sin \vartheta} \left( 1 - \frac{\cos \vartheta}{\sqrt{1 - \beta^2 \sin^2 \vartheta}} \right), \quad (\text{F30})$$

with respect to the coordinate system centered on  $B_z^-$ . The Berry curvature  $\vec{F}_-^{(S)}(dB, \vartheta, \phi)$  and  $\vec{\nabla} \times \vec{F}_-^{(S)}(dB, \vartheta, \phi)$  can then be calculated accordingly. The curl of the Berry curvature with respect to the original Cartesian coordinate system  $(B_x, B_y, B_z)$  takes then the form

$$\vec{\nabla} \times \vec{F}_{(\pm)}^{(C)} \approx -\frac{3}{2} \frac{\beta^2 B_x (B_z - B_z^{(\pm)})}{\gamma^2 [(1 - \beta^2) B_x^2 + (B_z - B_z^{(\pm)})^2]^{5/2}} \left( \frac{-B_y \hat{x} + B_x \hat{y}}{\sqrt{B_x^2 + B_y^2}} \right). \quad (\text{F31})$$

In the  $B_x - B_z$  plane, corresponding to  $B_y = 0$ , only the  $y$ -component of  $\vec{\nabla} \times \vec{F}_{(\pm)}^{(C)}$  is non-zero. This situation is

plotted in Fig. 11. For comparison we also plot the  $y$ -component of the curl of the Berry curvature calculated numerically by using exact diagonalization.

- 
- \* tsouza@bu.edu
- <sup>1</sup> C. L. Kane and E. J. Mele, Phys. Rev. Lett. **95**, 146802 (2005).
  - <sup>2</sup> B. A. Bernevig, T. L. Hughes, and S.-C. Zhang, Science **314**, 1757 (2006).
  - <sup>3</sup> M. König, S. Wiedmann, C. Brüne, A. Roth, H. Buhmann, L. W. Molenkamp, X.-L. Qi, and S.-C. Zhang, Science **318**, 766 (2007).
  - <sup>4</sup> D. Hsieh, D. Qian, L. Wray, Y. Xia, Y. S. Hor, R. J. Cava, and M. Z. Hasan, Nature (London) **452**, 970 (2008).
  - <sup>5</sup> M. V. Berry, Proc. R. Soc. London A **392**, 45 (1984).
  - <sup>6</sup> S. Oh, Phys. Lett. A, **373**, 644 (2009).
  - <sup>7</sup> S.-C. Li, L.-B. Fu, and J. Liu, Phys. Rev. A **89**, 023628 (2014).
  - <sup>8</sup> B. Wu, Q. Zhang, and J. Liu, Phys. Lett. A **375**, 545 (2011).
  - <sup>9</sup> J. Wiemer and F. Zhou, Phys. Rev. B **70**, 115110 (2004).
  - <sup>10</sup> E. Sjöqvist, R. Rahaman, U. Basu, and B. Basu, J. Phys. A: Math. Theor. **43**, 354026 (2010).
  - <sup>11</sup> D. Viennot, J. Math. Phys. **47**, 092105 (2006).
  - <sup>12</sup> A. I. Nesterov and F. Aceves de la Cruz, J. Phys. A: Math. Theor. **41**, 485304 (2008).
  - <sup>13</sup> P. Bruno, Phys. Rev. Lett. **96**, 117208 (2006).
  - <sup>14</sup> M. A. Nielsen and I. L. Chuang, *Quantum Computation and Quantum Information* (Cambridge University Press, Cambridge, U.K., 2000).
  - <sup>15</sup> P. Roushan, C. Neill, Y. Chen, M. Kolodrubetz, C. Quintana, N. Leung, M. Fang, R. Barends, B. Campbell, Z. Chen *et al.*, Nature (London) **515**, 241 (2014).
  - <sup>16</sup> X.-G. Wen, *Quantum Field Theory of Many-body Systems: From the Origin of Sound to an Origin of Light and Electrons* (Oxford University Press, New York, 2004).
  - <sup>17</sup> A. B. Bernevig and T. L. Hughes, *Topological Insulators and Topological Superconductors* (Princeton University Press, Princeton, NJ, 2013).
  - <sup>18</sup> V. Gritsev and A. Polkovnikov, Proc. Natl. Acad. Sci. U.S.A. **109**, 6457 (2012).
  - <sup>19</sup> J. E. Avron, M. Fraas, G. M. Graf, and O. Kenneth, New J. Phys. **13**, 053042 (2011).
  - <sup>20</sup> M. D. Schroer, M. H. Kolodrubetz, W. F. Kindel, M. Sandberg, J. Gao, M. R. Vissers, D. P. Pappas, A. Polkovnikov, and K. W. Lehnert, Phys. Rev. Lett. **113**, 050402 (2014).
  - <sup>21</sup> D. R. Yarkony, Acc. Chem. Res. **31**, 511 (1998).
  - <sup>22</sup> D. R. Yarkony, Rev. Mod. Phys. **68**, 985 (1996).
  - <sup>23</sup> J. W. Zwanziger and E. R. Grant, J. Chem. Phys. **87**, 2954 (1987).
  - <sup>24</sup> M. Nakahara, *Geometry, Topology and Physics* (Institute of Physics, London, 2003).
  - <sup>25</sup> D. J. Griffiths, *Introduction to Electrodynamics* (Prentice-Hall, Upper Saddle River, NJ, 1999).